Deformation banding under arbitrary monotonic loading in cubic metals

S. Mahesh* C. N. Tomé†

MST-8, Los Alamos National Laboratory, Los Alamos NM 87545.

Abstract

We present a Taylor-based theory of deformation of an aggregate of rigid-plastic crystals that allows for heterogeneity of grain deformation, and use it to model macroscopic subdivision of grains into mutually misoriented volumes, a process termed deformation banding. Each grain is assumed to accommodate the macroscopically imposed deformation such that the power of its plastic deformation is minimised. This minimisation may involve the formation of deformation bands. The theory is applied to tension, compression, and rolling of F.C.C. aluminium and B.C.C. α-iron polycrystals and used to predict the macroscopic mechanical response, the polycrystal texture, the orientation of deformation bands, and the misorientations across them. These predictions are compared with experimental observations available in the literature, and good qualitative agreement is found.

1 Introduction

Most polycrystal plasticity models assume that grains deform homogeneously within the aggregate. While this assumption is reasonably successful in predicting polycrystal behaviour

*ph: +1 505 667 8811, fax: +1 505 665 5926, email: mahesh@lanl.gov
†ph: +1 505 665 0892, fax: +1 505 667 8021, email: tome@lanl.gov

during plastic deformation, and in capturing the major texture components, it often results in quantitative and qualitative differences between the measured and calculated texture and flow response. For example, the predicted textures are systematically sharper than those measured, and certain experimentally observed texture components are not predicted (Lee and Duggan 1993). As a consequence, some researchers have started, in recent years, to incorporate more detailed descriptions of the dislocation structure and inhomogeneous grain deformation in their models (Peeters et al. 2001, Lee and Duggan 1993, Mahesh et al. 2004).

In this paper we propose a model for describing grain banding and evolution of misorientation, based on an energy minimization criterion. We apply this model to the simulation of tensile, compressive and plane strain deformation of polycrystalline aggregates of cubic structure. It is important to emphasize that our criterion is applicable to the 'mesoscopic' length scale, where the intergranular interactions control the deformation, and not to the 'microscopic' scale, where energy minimization taking place through dislocation rearrangement is driven by local stresses. The following discussion clarifies this point.

During plastic deformation, grains of cubic metals with medium to high stacking fault energy form relatively misoriented domains, each of which may undergo plastic deformation different from the grain average (Bay et al. 1992, Hughes and Hansen 1993). The subdivision into domains is effected over a wide range of length scales (see figure 1). The smallest subdivision is by incidental dislocation boundaries (IDBs) that arise from statistical trapping of glide dislocations. IDBs form dislocation cells and engender small lattice misorientations across themselves about a uniformly distributed random axis. On a larger length scale, geometrically necessary boundaries (GNBs) subdivide a grain by enclosing a group of cells, sometimes called a cell-block. GNBs form so as to accommodate deformation gradients in the flow field (Argon 2002, Dawson et al. 2002) and therefore, they tend to be preferentially oriented. The average misorientation across GNBs is larger than that across IDBs, and scales as a power law with grain strain (Hughes et al. 1997). Thus, commonly, IDBs separate lattice regions that have the same active slip systems deforming with different shear amplitudes,

while the domains separated by GNBs have differing slip system activities (Bay et al. 1992).

[Figure 1 about here.]

GNB structure displays considerable variety at any given strain, and also shows qualitative structural transitions with increasing strain. For reasons to be given below, a GNB structure of particular interest to this work is the deformation band (DB), visible even in optical micrographs of single crystals or large grained polycrystals (diameter $\gtrsim$ 100 μm, see figure 1). DB are the largest GNBs in such crystals, and enclose volumes only one or two orders of magnitude smaller than that of the grain itself. They have been described as 'slab-like' or 'lath' shaped alternating regions, that extend across the grain (i.e., terminate at grain boundaries (Kulkarni et al. 1998)). DBs are precursors of independent grains (Duggan and Lee 1996). The dislocation structure enclosing a DB may either be sharp or diffuse (Lee and Duggan 1993), and will be referred to as a deformation band boundary (DBB). If a DBB is diffuse and has width comparable to the DB itself, it has been called a transition band (Hansen and Jensen 1999, Liu and Hansen 1998). A smooth transition between the lattice orientations of adjacent DB is accomplished over the thickness of a DBB.

The number of DB in a grain has been found to be unvarying with applied strain (Lee et al. 1993, Liu and Hansen 1998). It is important that DBBs not be confused with the elongated 'lamellar boundaries' studied by Hughes and Hansen (1993): firstly, DBBs separate grain volumes much larger than those separated by lamellar boundaries, and secondly, grain subdivision into DBs takes place even at small strains (15% cold rolling of Al; see Liu and Hansen (1998)), whereas lamellar boundaries are characteristic of high strain sub-structures.

The definition of DB varies in the literature. Barrett (1939) and Barrett and Levenson (1940) studied the largest dislocation structures through optical microscopy in iron and aluminium, respectively, and coined the term *deformation bands* (DB) for the misoriented lattices. They also found 'fine structure' within the deformation bands, which have since been revealed as smaller dislocation structures using electron microscopy (Hughes and Hansen

1993). Although Barrett and Levenson applied the term 'deformation bands' to these smaller dislocation structures as well, later authors have primarily used it to denote macroscopic subdivision of grains. Our definition keeps with this later trend. We will call the largest dislocation structures, deformation band boundaries (DBBs), and the volumes they separate, deformation bands (DBs) if (i) they deform differently than the grain on average, and (ii) their minimum dimension is much larger than the mean free path of dislocations. Hansen and Jensen (1999) and Kuhlmann-Wilsdorf (1999*a*) have recently surveyed the phenomenon of deformation banding.

An energy criterion for the sub-structure formation was given by Chin and Wonsiewicz (1969). Loosely, it states that if the deformation energy or power can be sufficiently lowered by inhomogeneous grain deformation below that of homogeneous deformation, then the former will be favoured. Different authors have proposed different energies of deformation associated with this criterion. Lee and Duggan (1993), Lee et al. (1993), Ortiz and Repetto (1999), and Ortiz et al. (2000) have defined it as the *total* plastic work of deformation, and deformation banding in their models is a result of *latent hardening*. Kuhlmann-Wilsdorf's (1999*a*) model of deformation banding is similar to that of Chin and Wonsiewicz, except that instead of the plastic power, she considers the stored elastic strain energy as the quantity to be minimised.

Experimentally, much recent work has focused on the study of grain sub-structure that forms during plastic deformation over a range of imposed deformation conditions in both single and polycrystals (Huang and Hansen 1997, Winther et al. 1997, Christoffersen and Leffers 1998, Huang 1998, Winther et al. 2000, Wert 2002, Wert and Huang 2003). These works have focused on the length scale of the smallest GNB, i.e., at length scales comparable to the mean free path of dislocations (< 5 μm in aluminium deformed a few percent) and attempt to find patterns in the experimentally observed microstructure. However the phenomenological rules for the character of the microstructure that have emerged from these efforts are only applicable to certain specific deformation conditions on specific materials. No

simple general pattern of GNB position and orientation over arbitrary loading on arbitrarily oriented grains exists yet, nor is there an encompassing theory to explain the variations.

The energy-criterion mentioned above does not include dislocation kinetics, and cannot be expected to reliably predict GNB character at length scales comparable to the mean free path of individual dislocations. To see why, we recall Winther's (2003) observation that the microstructure at any length scale is influenced both by a 'crystallographic preference' and a 'macroscopic preference'. The crystallographic preference derives from the tendency of the dislocations available from slip activity to form local low energy dislocation structures (Kuhlmann-Wilsdorf 1999*b*), while the macroscopically preferred orientation is governed by macroscopic effects such as loading direction and grain orientation. DBBs being much larger than the dislocation mean free path, can be expected to be least influenced by the crystallographic preference, and form in a manner dominated by the macroscopic preference. As a consequence, the formation of 'macroscopic' DBBs can be studied separately from the 'microscopic' GNBs. DBs are also attractive from the perspective of polycrystal plasticity modelling because, being the largest dislocation structures, they are expected to have a greater influence on polycrystal texture and grain fragmentation than smaller misoriented volumes.

In this work, we restrict ourselves to modelling deformation banding, dominated by the macroscopic preference, and do not venture to model the competition between the crystallographic and macroscopic preferences to predict the orientations of GNB smaller than DB. In the following, we develop a theory of inhomogeneous grain deformation following the Chin-Wonsiewicz criterion, for rigid-plastic grains deforming according to the macroscopically imposed velocity gradient (Taylor polycrystal). In Section 2 we collect relevant facts about deformation banding from previous works. Section 3 details the theory, and Section 4 presents its predictions. Section 5 discusses these results and compares them with previous theories.

2 Previous work on deformation banding

Experimental work on DB has been done both on polycrystals and on single crystals. Barrett (1939) and Barrett and Levenson (1940) first recognised the inhomogeneity of grain deformation in mild steel and aluminium, respectively, and ruled out twinning as its cause. More recently, Lee, Duggan, and co-workers have extensively studied deformation banding during cold rolling of F.C.C. copper polycrystals (Lee and Duggan 1993, Lee et al. 1993, Lee et al. 1995) and Duggan and co-workers have studied B.C.C. steel (Tse et al. 2000, Liu and Duggan 2001). They observe a three-dimensional arrangement of lath-shaped DB, each spanning the length of the grain in the longitudinal section.

An experimental deformation banding study during uniaxial compression of aluminium was carried out by Kulkarni et al. (1998). They observe primary, secondary, and even tertiary DB, nested within each other, and a grain size dependence of the number of bands.

Akef and Driver (1991), Maurice and Driver (1993), and Basson and Driver (2000) have conducted detailed experimental studies of the deformation banding of cube oriented F.C.C. *single crystals* subjected to channel-die compression. They find that depending on the metal, deformation bands form after a certain amount of strain, with the DBBs perpendicular to the transverse direction (TD). Using the Bishop-Hill crystal plasticity theory, they explain the rotations of the deformation bands (after their formation) as due to spatial separation of the slip system activity needed to accommodate the imposed deformation. An important observation of these authors is that once bands form, they rapidly rotate about the TD relative to each other. In the nominally identical plane strain loading under rolling, Liu and Hansen (1998), and Liu et al. (2000) have studied the development of macroscopic misorientations in cube oriented aluminium single crystals. Although they too find that bands rotate about the TD, their DBBs form perpendicular to the normal direction (ND). They ascribed the observed misorientation development to location dependent shear stresses (Lee and Duggan 1991) imposed during rolling deformation.

On the theoretical side, an energy based criterion for the formation of deformation bands was proposed by Chin and Wonsiewicz (1969) to explain the phenomenon observed experimentally (Ahlborn 1966, Ahlborn 1966b) in axisymmetric wire drawing. Their framework has been retained by all succeeding authors, and indeed, underlies the present work. Expressed in terms of deformation rates instead of infinitesimal deformation increments, it states that a grain will band during plastic deformation if the power required to accomplish a certain shape change by homogeneous deformation, $\dot{W}_H = \sum_s \tau_s \dot{\gamma}_s$ exceeds that by banded deformation. Here τ_s and $\dot{\gamma}_s$ denote the critical resolved shear stress and the slip strain rate on slip system s, respectively. The latter power consists of 1) $\dot{W}_i$, the power of slip within the bands, 2) $\dot{W}_b$, the power associated with formation of boundary between bands, and 3) $\dot{W}_c$, power to correct the difference in shape arising from banding and homogeneous deformation. Thus, the Chin-Wonsiewicz condition for grain banding is that

$$\dot{W}_B = \dot{W}_i + \dot{W}_b + \dot{W}_c < \dot{W}_H. \tag{1}$$

Chin and Wonsiewicz did not compute $\dot{W}_b$ and $\dot{W}_c$. However, they show that Ahlborn's experimental observations satisfy $\dot{W}_i < \dot{W}_H$ which is necessary if Eq. (1) is to be satisfied.

In their model of deformation banding, Lee and Duggan (1993) and Lee et al. (1993) minimise the internal *work* of plastic deformation, over finite deformation steps. Their model grains experience latent hardening on all non-primary slip planes. If $\Delta\gamma_s$ is the deformation increment over a finite deformation step on slip system s, τ_s the critical resolved shear stress (CRSS) at the beginning of that step, and $h_{ss'}$ the latent hardening coefficient between slip systems s and s', then the average CRSS over that step is $\tau_s + (1/2)\sum_{s'} h_{ss'}\Delta\gamma_{s'}$. Thus, the work of incremental plastic deformation is

$$\Delta W = \sum_s \tau_s \Delta\gamma_s + (1/2)\sum_s \sum_{s'} h_{ss'}\Delta\gamma_s\Delta\gamma_{s'}. \tag{2}$$

In their model, latent hardening drives deformation banding, since slip on multiple planes may be avoided in different bands while still accommodating the imposed deformation on average over all bands. This way, the otherwise large work of deformation due to latent hardening can be lowered by suppressing latent hardening in individual bands. The minimisation in Lee and Duggan's model is carried out subject to the constraint that DBBs are oriented perpendicular to the TD. They fix the extensional strains in both DBs to be the same as that of the grain, but relax the shear strain components in each DB in the planes perpendicular to the TD and rolling direction (RD) using relaxed constraints (RC). They then require that the shear strain components in the plane perpendicular to ND cancel out between the two sub-grains. They also compute the accommodation energy W_b in the Chin-Wonsiewicz condition using Read and Shockley's (1950) formula of the surface energy associated with a low-angle grain boundary and W_c as the elastic energy stored due to forcing displacement compatibility at the ends of flat deformation bands aligned with the rolling direction. Using this theory, they find that increasing numbers of grains band with continued deformation. They also find that the formation of bands is sensitive to the grain orientation relative to loading.

The theory of Ortiz and Repetto (1999), and Ortiz et al. (2000) extends that of Lee and Duggan by removing many of the restrictive assumptions. It allows for the formation of nested deformation bands, arbitrary DBB orientation and arbitrary monotonic loading paths. The accommodation terms are treated quite differently than in the theory and Lee et al. In Ortiz et al's theory too, latent hardening drives microstructuring; its absence will result in homogeneous deformation.

The minimisation of ΔW in Eq. (2) inherently involves 'looking ahead' in the deformation by a finite $\Delta\gamma_s$ to determine whether it would be energetically beneficial to band or not at a certain instant during the deformation. It is essential that $\Delta\gamma_s$ be non-infinitesimal in order that the second term in Eq. (2) influence ΔW. For, in the limit $\Delta\gamma_s \downarrow 0$, the second term scales as a quadratic in $\Delta\gamma_s$ and diminishes more rapidly than the linearly diminishing first

term in Eq. (2). In this limit, the above theories predict no deformation banding. Thus, in addition to the physical grain's dislocation substructure at a certain instant (as indirectly quantified by the CRSS of its slip systems), its deformation banding criterion according to the above theories seemingly involves foresight of its future deformation.

It should be emphasised that the validity of the above theories or of their energy criteria is not being questioned here. Latent hardening in these theories is used simply as an abstract *model* of the experimental fact that grains prefer to use a smaller number of slip systems, and is not to be viewed as advance knowledge supplied to the grain on its forthcoming deformation. Nevertheless, in our view, a theory that supplies a *physical mechanism* for lowering the number of active slip systems involving only the present state of the grain, without recourse to its future deformation would be more physically grounded. Such a mechanism (which naturally cannot hinge on latent hardening, but which does not exclude latent hardening either) and theory of deformation banding will be presented next. The key idea is that macroscopic DBs are assumed to be 'seeded' by misorientation across IDBs, which may develop into substantially misoriented GNBs if doing so is energetically favourable. It will turn out that the number of active slip systems in each band will reduced from the number needed in homogeneous deformation, just as in the theory of Lee and Duggan. On a different line, we also note here that the deformation banding criterion does not hinge on (but does not forbid either) rate sensitivity of the grain constitutive law.

3 The deformation banding theory

3.1 Assumptions

We collect some definitions and assumptions regarding the deformation of individual grains and their interaction with each other in a polycrystal here.

Consider a grain, each of whose S slip system orientations have unit normal $\mathbf{n}^s$, and

Burgers vector $\mathbf{b}^s$. The Schmid tensor ($\mathbf{m}^s$, $s = 1, \ldots, S$) is given by (Kocks et al. 1998)

$$\mathbf{m}^s = (\mathbf{n}^s \otimes \mathbf{b}^s + \mathbf{b}^s \otimes \mathbf{n}^s)/2. \tag{3}$$

If $\dot{\gamma}^s$ denotes the slip rate on slip system s, $s = 1, 2, \ldots, S$, then the velocity gradient is

$$\mathbf{L} = \sum_{s=1}^{S} \dot{\gamma}^s \mathbf{b}^s \otimes \mathbf{n}^s, \tag{4}$$

and the strain rate tensor in the grain is given by

$$\dot{\boldsymbol{\epsilon}} = \sum_{s=1}^{S} \dot{\gamma}^s \mathbf{m}^s = \text{sym } \mathbf{L}. \tag{5}$$

The deformation gradient $\mathbf{F}$ of the grain has a rate of change (Gurtin 1981) given by

$$\dot{\mathbf{F}} = \mathbf{L}\mathbf{F}. \tag{6}$$

In an incremental implementation of crystal plasticity, as done in the present work, Eq. (6) is used to generate a linear extrapolation of the deformation gradient of the grain. Let $\mathbf{L}^k$, and $\mathbf{F}^k$ be the velocity and deformation gradients at time step k, and let t_k be the time of the k-th increment (Kocks et al. 1998). Then,

$$\mathbf{F}^{k+1} = \mathbf{F}^k + (t_{k+1} - t_k)\mathbf{L}^k\mathbf{F}^k \tag{7}$$

represents a good approximation of $\mathbf{F}^{k+1}$ for small $t_{k+1} - t_k$.

Throughout, we ignore elastic deformations; the grain constitutive response is assumed to be rigid-plastic following the viscoplastic constitutive law proposed by Hutchinson (1976),

Asaro and Needleman (1985), and Canova et al. (1988):

$$\dot{\gamma}^s = \left| \frac{\boldsymbol{\sigma} : \mathbf{m}^s}{\tau^s} \right|^n \operatorname{sign}(\boldsymbol{\sigma} : \mathbf{m}^s), \quad s = 1, 2, \ldots, S. \tag{8}$$

$\boldsymbol{\sigma}$ is the *deviatoric* stress experienced by the grain, $\tau^s > 0$ is the critical resolved shear stress on slip system s, and n the reciprocal of the rate sensitivity. As $n \uparrow \infty$, the material becomes rate-insensitive. We will assume $n > 2$. Using Eqs. (5) and (8), we get

$$\dot{\boldsymbol{\epsilon}} = \sum_{s=1}^{S} \mathbf{m}^s \left| \frac{\boldsymbol{\sigma} : \mathbf{m}^s}{\tau^s} \right|^n \operatorname{sign}(\boldsymbol{\sigma} : \mathbf{m}^s). \tag{9}$$

Since the symmetric $\dot{\boldsymbol{\epsilon}}$ denotes the plastic strain rate, it is volume preserving so that Tr $\dot{\boldsymbol{\epsilon}} = 0$. Thus, $\dot{\boldsymbol{\epsilon}}$ can be fully specified using 5 independent coordinates, and we will use the Leibfried and Breuer representation (Kocks et al. 1998, Chap. 7) of $\dot{\boldsymbol{\epsilon}}$ as a 5-tuple. It is important to note that this representation is basis-dependent i.e., it does not transform tensorially. In this scheme, $[\dot{\boldsymbol{\epsilon}}] = \dot{\epsilon}_{ij}$ has the representation

$$\{\dot{\epsilon}_\lambda\} = \left\{ \frac{\dot{\epsilon}_{22} - \dot{\epsilon}_{11}}{\sqrt{2}}, \ \frac{2\dot{\epsilon}_{33} - \dot{\epsilon}_{22} - \dot{\epsilon}_{11}}{\sqrt{6}}, \sqrt{2}\dot{\epsilon}_{23}, \sqrt{2}\dot{\epsilon}_{13}, \sqrt{2}\dot{\epsilon}_{12} \right\} \tag{10}$$

and $[\boldsymbol{\sigma}] = \sigma_{ij}$ the representation

$$\{\sigma_\lambda\} = \left\{ \frac{\sigma_{22} - \sigma_{11}}{\sqrt{2}}, \ \frac{2\sigma_{33} - \sigma_{22} - \sigma_{11}}{\sqrt{6}}, \sqrt{2}\sigma_{23}, \sqrt{2}\sigma_{13}, \sqrt{2}\sigma_{12} \right\} \tag{11}$$

where $\lambda = 1, 2, \ldots, 5$. The summation convention over repeated indices will be used, except when the index identifies a slip system.

3.2 The banding condition

Except for the work of Lee, Duggan and co-workers, the Chin-Wonsiewicz condition has only been used to verify that Eq. (1) holds in particular experimentally observed banding

grains. Lee and Duggan (1993) were the first to calculate the band deformations as those that minimise $\dot{W}_B$, subject to the constraint that the imposed grain deformation is accommodated on average by the bands. Lee et al. (1995) later observed that $\min \dot{W}_i < \dot{W}_H$ very likely implies $\min \dot{W}_B < \dot{W}_H$.

We presently give a formula for the terms in $\dot{W}_B$, and describe a simplified approximate methodology to compute $\min \dot{W}_B$, by sequentially minimising $\dot{W}_i$, and then $\dot{W}_b + \dot{W}_c$. The negligibility of $\dot{W}_b + \dot{W}_c$ compared to $\dot{W}_i$, which justifies this approximation, was observed by Lee et al. (1995). We will show *a posteriori* that in the present calculation also, sequential minimisation of $\dot{W}_B$ should result in no significant errors.

3.2.1 Plastic power ($\dot{W}_i$)

Consider a grain on which strain rate $\dot{\boldsymbol{\epsilon}}^G$ is imposed. The corresponding stress $\boldsymbol{\sigma}^G$ is given by the viscoplastic constitutive law Eq. (9). The plastic power of the grain under homogeneous deformation $\dot{W}_H$ is then

$$\dot{W}_H(\dot{\boldsymbol{\epsilon}}^G) = \boldsymbol{\sigma}^G : \dot{\boldsymbol{\epsilon}}^G = \sum_{s=1}^{S} \tau_s \left| \frac{\boldsymbol{\sigma}^G : \mathbf{m}^s}{\tau^s} \right|^{n+1} = \sum_{s=1}^{S} \tau^s |\dot{\gamma}^s|^{1+1/n}. \tag{12}$$

To simplify consideration of inhomogeneous deformation under an imposed $\dot{\boldsymbol{\epsilon}}^G$, we model the grain as a pair of bands, each of which has the same lattice orientation as the original (homogeneously deforming) grain. Let the pair of bands have volume fractions w and $1-w$ relative to the grain volume, $0 \leq w \leq 1$. If $\dot{\boldsymbol{\epsilon}}^{(1)}$ and $\dot{\boldsymbol{\epsilon}}^{(2)}$ are the strain rates of each of the bands, then the full constraints condition (Hill 1967) requires that

$$w\dot{\boldsymbol{\epsilon}}^{(1)} + (1-w)\dot{\boldsymbol{\epsilon}}^{(2)} = \dot{\boldsymbol{\epsilon}}^G. \tag{13}$$

If the stresses corresponding to $\dot{\boldsymbol{\epsilon}}^{(1)}$ and $\dot{\boldsymbol{\epsilon}}^{(2)}$ computed according to Eq. (9) are $\boldsymbol{\sigma}^{(1)}$ and $\boldsymbol{\sigma}^{(2)}$, respectively, then the plastic power of banded deformation is

$$\dot{W}_i(w, \dot{\boldsymbol{\epsilon}}^{(1)}, \dot{\boldsymbol{\epsilon}}^{(2)}) = w\boldsymbol{\sigma}^{(1)} : \dot{\boldsymbol{\epsilon}}^{(1)} + (1-w)\boldsymbol{\sigma}^{(2)} : \dot{\boldsymbol{\epsilon}}^{(2)}. \tag{14}$$

In applying Eq. (9) to compute $\boldsymbol{\sigma}^{(1)}$ and $\boldsymbol{\sigma}^{(2)}$ given $\dot{\boldsymbol{\epsilon}}^{(1)}$ and $\dot{\boldsymbol{\epsilon}}^{(2)}$, respectively, we assume that τ^s, and $\mathbf{m}^s$, $s = 1, \ldots, S$ in both bands have the same value as that in the homogeneous grain. It should be noted that the domain undergoing deformation with strain rate $\dot{\boldsymbol{\epsilon}}^{(1)}$ or $\dot{\boldsymbol{\epsilon}}^{(2)}$ need not be contiguous for Eq. (14) to hold. In fact, we will later regard the grain subdivided as shown in figure 2, consisting of bands alternately deforming with strain rate $\dot{\boldsymbol{\epsilon}}^{(1)}$ and $\dot{\boldsymbol{\epsilon}}^{(2)}$. It is only important for the validity of Eq. (14) that the volume fraction of all bands deforming with strain rate $\dot{\boldsymbol{\epsilon}}^{(1)}$ add up to w, and those deforming with $\dot{\boldsymbol{\epsilon}}^{(2)}$ add up to $1-w$.

[Figure 2 about here.]

Now, $\dot{W}_H(\dot{\boldsymbol{\epsilon}}^G)$ in Eq. (12) is convex in $\dot{\boldsymbol{\epsilon}}^G$ (Ortiz and Repetto 1999), i.e., given any strain rates $\dot{\boldsymbol{\epsilon}}^{(1)}$, and $\dot{\boldsymbol{\epsilon}}^{(2)}$ satisfying Eq. (13),

$$\begin{gathered}\dot{W}_i(w, \dot{\boldsymbol{\epsilon}}^{(1)}, \dot{\boldsymbol{\epsilon}}^{(2)}) = w\dot{W}_H(\dot{\boldsymbol{\epsilon}}^{(1)}) + (1-w)\dot{W}_H(\dot{\boldsymbol{\epsilon}}^{(2)}) \geq \\ \dot{W}_H(w\dot{\boldsymbol{\epsilon}}^{(1)} + (1-w)\dot{\boldsymbol{\epsilon}}^{(2)}) = \dot{W}_H(\dot{\boldsymbol{\epsilon}}^G),\end{gathered} \tag{15}$$

which rules out satisfaction of the Chin-Wonsiewicz condition, Eq. (1).

The convexity of $\dot{W}_H(\dot{\boldsymbol{\epsilon}}^G)$ however, is broken if the bands are mutually misoriented. To describe the misorientation, we let the misorientation angle between the bands be $2\omega_m$ about an axis given by the unit vector

$$\hat{\mathbf{m}} = (\sin\theta_m \cos\phi_m, \ \ \sin\theta_m \sin\phi_m, \ \ \cos\phi_m). \tag{16}$$

The Schmid tensor $\mathbf{m}^s$, for each s of the first band is assumed rotated by an angle $+\omega_m$ relative to the s-th Schmid tensor of the original (homogeneously deforming) grain, while that of the second band is assumed rotated by $-\omega_m$, about $\hat{\mathbf{m}}$. The critical resolved shear stress τ_s is however assumed to be the same for each s in each band as that in the original grain.

The physical phenomenon idealised by the misorientation ω_m is the misorientation across IDBs that accompany plastic deformation. Hughes et al. (1997) found that the average misorientation across IDBs, ω_{av} scales with grain von Mises strain ϵ_{vM} as

$$\omega_{\text{av}} = k_\omega \epsilon_{\text{vM}}^\nu, \tag{17}$$

where empirical exponent values of $\nu = 0.5$ for cold rolled pure aluminium (Hughes et al. 1997), and $\nu = 0.4$ for commercial purity aluminium (Liu et al. 2002) have been reported and k_ω ($\approx 1^\circ$ for aluminium) is the scaling constant. They also find that misorientation axes corresponding to IDBs are uniformly distributed over all possible directions. Furthermore, Hughes et al have also found experimentally that the statistical distribution of misorientation angles has a heavy upper tail, i.e., misorientation angles four or five times the average ω_{av} are rare, but do occur.

We thus regard IDBs as *misorientation seeds*. The idea behind the present criterion of grain banding is that of all IDBs, an energetically optimal IDB will be favoured to form a DBB that may, with further deformation, develop large misorientation across itself. Since IDB misorientation axes are uniformly distributed over all possible directions, finding the energetically optimal IDB amounts to finding a misorientation axis, and a misorientation angle (within bounds) at which $\dot{W}_i$ is minimised.

We will now describe the minimisation procedure for $\dot{W}_i$. Given $\dot{\boldsymbol{\epsilon}}^G$, for fixed w, θ_m, ϕ_m, and ω_m, different choices of $(\dot{\boldsymbol{\epsilon}}^{(1)}, \dot{\boldsymbol{\epsilon}}^{(2)})$ satisfying Eq. (13) will result in different $\dot{W}_i$ according to Eq. (14). Appendix A however shows that of all such choices, that choice of $(\dot{\boldsymbol{\epsilon}}^{(1)}, \dot{\boldsymbol{\epsilon}}^{(2)})$

satisfying Eq. (13) will minimise $\dot{W}_i$ which, in addition, satisfies

$$\boldsymbol{\sigma}^{(1)} = \boldsymbol{\sigma}^{(2)}. \tag{18}$$

Since we wish to minimise $\dot{W}_i$, we restrict ourselves to this case only. Then, defining $\boldsymbol{\sigma}^G := \boldsymbol{\sigma}^{(1)} = \boldsymbol{\sigma}^{(2)}$, $\dot{W}_i$ can be written as

$$\begin{aligned} \dot{W}_i(w, \theta_m, \phi_m, \omega_m) &= \boldsymbol{\sigma}^G : (w\dot{\boldsymbol{\epsilon}}^{(1)} + (1-w)\dot{\boldsymbol{\epsilon}}^{(2)}) = \boldsymbol{\sigma}^G : \dot{\boldsymbol{\epsilon}}^G \\ &= w \sum_{s=1}^{S} \tau_s \left| \frac{\boldsymbol{\sigma}^G : \mathbf{m}^{s,(1)}}{\tau^s} \right|^{n+1} + (1-w) \sum_{s=1}^{S} \tau_s \left| \frac{\boldsymbol{\sigma}^G : \mathbf{m}^{s,(2)}}{\tau^s} \right|^{n+1}. \end{aligned} \tag{19}$$

Here $\mathbf{m}^{s,(1)}$ and $\mathbf{m}^{s,(2)}$ represent the s-th Schmid tensor (Eq. (3)) of each of the two bands rotated relative to the original grain by $\pm\omega_m$ about $\hat{\mathbf{m}}$.

Let $\dot{W}_i^*$ denote the minimum banded power of a grain:

$$\dot{W}_i^* = \min_{w, \theta_m, \phi_m, \omega_m} \dot{W}_i(w, \theta_m, \phi_m, \omega_m), \tag{20}$$

subject to the constraints Eq. (13), Eq. (18), and,

$$\begin{aligned} 0 \leq \omega_m &\leq r\omega_{\text{av}}, \\ 0 \leq \theta_m, \phi_m &\leq \pi. \end{aligned} \tag{21}$$

We implement the minimisation of Eq. (20) using a standard gradient-based constrained optimisation package (Spellucci 1998). Although the analytical computation of the gradients $\partial\dot{W}_i/\partial w$, $\partial\dot{W}_i/\partial\theta_m$, $\partial\dot{W}_i/\partial\phi_m$, and $\partial\dot{W}_i/\partial\omega_m$, is tedious, it proves computationally advantageous over numerical differentiation for the gradients.

The first constraint in Eq. (21) expresses the fact that misorientations across IDBs are usually fairly small, and grow with strain according to Eq. (17). $r \geq 1$ denotes a factor by which the misorientation angle at band inception is allowed to exceed the average misori-

entation angle as given by Eq. (17). As already noted, the upper tail of the misorientation distribution is found to be heavy, and r denotes the ratio of the maximum allowable misorientation to the average misorientation. The bounds on θ_m, and ϕ_m simply restrict the misorientation axis to one half plane. They can be narrowed further by accounting for lattice symmetry.

A degenerate minimum, often achieved, arises at $w = 0$ or $w = 1$. Physically this corresponds to the situation that $\min \dot{W}_i$ is achieved by rotating the entire grain by ω_m about some misorientation axis $\hat{\mathbf{m}}$. For grains embedded in a polycrystal, we rule out such rotations on physical grounds, and take the banding criterion as having failed in this case. Even in the absence of this degeneracy, we disallow the grain from being dominated by one band. For a fixed $0 \leq c < 0.5$, we take the banding condition as having failed unless $c < w < 1 - c$. We take $c = 0.2$, and thus ensure that the smaller band at least occupies 20% of the grain volume.

Note that homogeneous deformation is one of the states of the banded strain over which minimisation is done: It corresponds to $\omega_m = 0$. If the minimum is achieved away from the homogeneous deformation state, and is not degenerate, it implies that banding does indeed lower the plastic power of deformation below that of homogeneous deformation.

[Figure 3 about here.]

In the case of deformation paths such as rolling, which lead to the progressive flattening of grains, it has been argued (see e.g., Hosford (1993, Chap. 6)) that the full constraints (FC) condition, Eq. (13) may be unrealistic. A better approximation of the imposed deformation, it is argued, is provided by relaxing the shear strain components whose complementary stresses shear the flat surfaces of the grain. Thus, if as shown in figure 3, $\mathbf{n}_{\mathrm{RC}}$ denotes the normal to the flat surface of the grain and parallel to the sample coordinate system's

2-direction, the strain rate components $\dot{\epsilon}_3 = \dot{\epsilon}_{12}$ and $\dot{\epsilon}_5 = \dot{\epsilon}_{23}$ are relaxed by writing

$$\begin{aligned} w\dot{\epsilon}_i^{(1)} + (1-w)\dot{\epsilon}_i^{(2)} &= \dot{\epsilon}_i^G, i = 1, 2, 4, \\ w\sigma_i^{(1)} + (1-w)\sigma_i^{(2)} &= \sigma_i^G, i = 3, 5, \end{aligned} \tag{22}$$

instead of Eq. (13). It turns out that Eq. (18) holds true under the imposed relaxed constraints (RC) deformation given by Eq. (22) also, provided $\sigma_3^G = \sigma_5^G = 0$. Thus the minimisation in Eq. (20) is still applicable to RC, although the details of its implementation are different from that in FC.

3.2.2 Accommodation power ($\dot{W}_b + \dot{W}_c$)

In the case that $\dot{W}_i^*$ is attained in a state of banded deformation, the above procedure yields $\dot{\boldsymbol{\epsilon}}^{(1)}$, $\dot{\boldsymbol{\epsilon}}^{(2)}$, $\boldsymbol{\sigma}^{(1)} = \boldsymbol{\sigma}^{(2)}$ and w of the DB, and the misorientation axis $\hat{\mathbf{m}}$ and angle ω_m of the DBB. DBB orientation however is not given by this minimisation. Note that since stress is uniform, equilibrium is fulfilled across every plane in the grain. However, in general, the DB deformations will not be compatible. That is, if $\mathbf{L}^{(1)}$, and $\mathbf{L}^{(2)}$, are DB velocity gradients (from Eq. (4), where $\dot{\gamma}^s$ are given by Eq. (8)), the condition for compatibility (Hill 1961) is that there exist a vector $\mathbf{a}$ such that

$$\mathbf{L}^{(1)} - \mathbf{L}^{(2)} = \mathbf{a} \otimes \mathbf{n}. \tag{23}$$

This condition is not satisfied in general.

Incompatibility also occurs due to banding at the grain boundary. As shown in figure 2, inhomogeneity in grain bulk deformation may alter its surface profile leading to incompatibility with neighbouring grains. Thus, although compatible deformation across grain boundaries is guaranteed in a Taylor polycrystal with homogeneously deforming grains, grain boundary accommodation will be needed if banding is allowed.

Following Ashby (1970), we will assume that compatibility is restored by local inhomo-

geneous deformations close to the DBB and grain boundaries, thereby generating geometrically necessary dislocations (GND). We take the energy stored in DBBs to be Chin and Wonsiewicz's $\dot{W}_b$, and the stored energy at the grain boundary to be their $\dot{W}_c$ (see Eq. (1)). The complexity of the highly inhomogeneous accommodation processes at these boundaries precludes accurate computation of these terms. An order of magnitude estimate is however possible and detailed in Appendix B. According to this estimate,

$$\dot{W}_b = \kappa_b \frac{N\alpha G b}{D} \|[\mathbf{L}_0]\mathbf{F}_0 \times \mathbf{n}\|, \tag{24}$$

and,

$$\dot{W}_c = \frac{N}{2} \frac{\alpha G b \delta_c}{D^2} \|[\mathbf{L}_0]\mathbf{F}_0\|. \tag{25}$$

Here, $[\mathbf{L}_0]$ is the jump in the velocity gradient of the grain parallel to the DBB normal $\mathbf{n}$, and $\mathbf{F}_0$ the deformation gradient of the (hitherto homogeneously deforming) grain at the instant of banding. D is the diameter of the grain, G, the shear modulus, b the magnitude of Burgers vector, α a dislocation interaction parameter, and N the number of DBBs. κ_b is an unknown factor of the order of one to compensate for the approximations employed in deriving the above expressions, and δ_c the thickness of the accommodation layer at the grain boundary.

δ_c has been discussed by Meyers and Ashworth (1982). They suggest that δ_c may be a function of grain diameter, and suggest the power law dependence: $\delta_c \sim D^m$. In a banded grain with N bands, since the smallest dimension of each band is of the order of (D/N), it seems reasonable to take $\delta_c \sim (D/N)^m$. For reasons to become clear below Eq. (30), we assume

$$\delta_c = \kappa_c \left(\frac{D}{D_0 N} \right)^2, \tag{26}$$

where D_0 is a reference diameter, and κ_c/D_0^2 is a scaling constant. Then, Eq. (25) becomes

$$\dot{W}_c = \frac{\kappa_c \alpha G b}{2 D_0^2 N} \|[\mathbf{L}_0]\mathbf{F}_0\|. \tag{27}$$

The term $\dot{W}_b$ depends on the orientation of the band interface normal $\mathbf{n}$, while $\dot{W}_c$ does not. We hypothesise that $\mathbf{n}$ is so as to minimise $\dot{W}_b$. This entails a minimisation in the two-dimensional space of (θ_n, ϕ_n) if $\mathbf{n}$ were parametrized as

$$\mathbf{n} = [\sin\theta_n \cos\phi_n, \quad \sin\theta_n \sin\phi_n, \quad \cos\phi_n]^T. \tag{28}$$

So far, N has been left undetermined. Lee and Duggan (1993) suggest that the number of bands will be so as to minimise the total power of accommodation $\dot{W}_b + \dot{W}_c$ at the instant of banding. ($\dot{W}_i$ is independent of N.) Temporarily regarding N as continuous variable and setting

$$\frac{d(\dot{W}_b + \dot{W}_c)}{dN} = 0 \tag{29}$$

yields

$$N = \sqrt{D} \sqrt{\frac{\kappa_c}{2\kappa_b D_0^2} \frac{\|[\mathbf{L}_0]\mathbf{F}_0\|}{\|[\mathbf{L}_0]\mathbf{F}_0 \times \mathbf{n}\|}}. \tag{30}$$

The square root scaling $N \sim \sqrt{D}$ was derived by Lee et al. (1993) using completely different physical arguments, and different expressions for $\dot{W}_b$ and $\dot{W}_c$. Underlying our derivation of this relation is the power law assumption in Eq. (26). For any powers smaller than $m = 2$, the optimal number of bands would be $N = 0$; for powers larger than $m = 2$, other scaling relations will follow. Thus the presently chosen $m = 2$ represents the smallest exponent in Eq. (26) for which banding is possible. To render N an integer, we round down the value calculated using Eq. (30). The banding condition is taken to fail if $N = 0$.

With respect to N, the present model follows the viewpoint of Lee et al. (1993) in assuming that N is determined at the instant of banding, and does not evolve with further

deformation. In contrast, the model of Ortiz et al. (2000) subdivides grains into $N = 2$ bands, these bands being allowed to divide with further deformation. However, it is easy to see a synthesis of these two viewpoints, with grains banding into N (not necessarily equal to two) bands according to Lee et al.'s (1993) idea, and these bands refining further according to the model of Ortiz et al. (2000).

In summary, the banding condition involves performing the minimisation given by Eq. (20). If the minimum is achieved in a non-degenerate state of inhomogeneous deformation, and the reduction in deformation power exceeds the power of accommodation, Eqs. (24,25), the grain is theorised to band. If any of these tests fail, the grain is assumed to continue deforming homogeneously. The deformation banding test is carried out at every strain increment in our incremental implementation of polycrystal plasticity.

3.3 Deformation of a banded grain

The preceding Section 3.2 was concerned with a criterion for the formation of DB. The further deformation of a grain, once banded, will be discussed here.

According to the Taylor theory of homogeneously deforming grains, the activation of slip systems for a given imposed deformation occurs so as to minimise the plastic power $\dot{W}_H$ in Eq. (12) (Chin and Mammel 1969). This notion is directly extensible to the inhomogeneous deformation case: the inhomogeneous plastic power given by Eq. (14) should be minimised subject to the constraint Eq. (13) that the imposed deformation on the grain be satisfied. As already discussed, this minimum occurs when Eq. (18) is satisfied. Thus explicitly, given $\dot{\boldsymbol{\epsilon}}^G$, the twenty algebraic equations to be solved for determining the deformation in a banded

grain as described by the twenty components of $\dot{\boldsymbol{\epsilon}}^{(1)}$, $\dot{\boldsymbol{\epsilon}}^{(2)}$, $\boldsymbol{\sigma}^{(1)}$, and $\boldsymbol{\sigma}^{(2)}$ are

$$\begin{aligned} \dot{\boldsymbol{\epsilon}}^{G} &= w\dot{\boldsymbol{\epsilon}}^{(1)} + (1-w)\dot{\boldsymbol{\epsilon}}^{(2)}, \\ \boldsymbol{\sigma}^{(1)} &= \boldsymbol{\sigma}^{(2)}, \quad \text{and} \\ \dot{\boldsymbol{\epsilon}}^{(i)} &= \sum_{s=1}^{S} \mathbf{m}^{s,(i)} \left| \frac{\boldsymbol{\sigma}^{(i)} : \mathbf{m}^{s,(i)}}{\tau^{s,(i)}} \right|^{n} \operatorname{sign}(\boldsymbol{\sigma}^{(i)} : \mathbf{m}^{s,(i)}), \qquad i = 1, 2. \end{aligned} \tag{31}$$

Here $\mathbf{m}^{s,(1)}$, and $\mathbf{m}^{s,(2)}$ refer to the Schmid tensors of the s-th slip system in the first and second band, respectively, and $\tau^{s,(1)}$, and $\tau^{s,(2)}$ to their critical resolved shear stresses. In minimising the power of deformation, the power of accommodation of incompatibly deforming bands is taken to be negligible in comparison to the plastic power.

Once a grain bands, we assume that the volume fraction of each band, w, and $1-w$ are fixed thereafter, i.e., the DBB has no mobility relative to the bands. As for the orientation of the DBB, we assume that it rotates with the grain shape (not lattice). That is, if the band forms with normal $\mathbf{n}_0$ when the grain deformation gradient is $\mathbf{F}_0$, the normal $\mathbf{n}$ when the deformation gradient is $\mathbf{F}$, will be

$$\mathbf{n} = \mathbf{F}_0^T \mathbf{F}^{-T} \mathbf{n}_0 / \| \mathbf{F}_0^T \mathbf{F}^{-T} \mathbf{n}_0 \|. \tag{32}$$

To see this, consider two vectors $\mathbf{a}$ and $\mathbf{b}$ in the plane of the band interface (i.e., parallel to the DBB) at the instant of banding when the grain deformation gradient is $\mathbf{F}_0$. $\mathbf{n}_0$ is thus parallel to $\mathbf{a} \times \mathbf{b}$. The deformation gradient of the transformation from this state to the final deformation gradient of $\mathbf{F}$ is ${\mathbf{F}_0}^{-1}\mathbf{F}$. Under this transformation $\mathbf{a} \times \mathbf{b}$ maps to $({\mathbf{F}_0}^{-1}\mathbf{F}\mathbf{a}) \times ({\mathbf{F}_0}^{-1}\mathbf{F}\mathbf{b})$. Now, using the identity (Gurtin 1981, p. 53) $\mathbf{S}\mathbf{a} \times \mathbf{S}\mathbf{b} = \det(\mathbf{S})\mathbf{S}^{-T}(\mathbf{a} \times \mathbf{b})$, it is seen that the unit normal to the banded plane is the unit vector parallel to $\mathbf{F}_0^T \mathbf{F}^{-T}(\mathbf{a} \times \mathbf{b})$.

The preceding assumptions of 1) continuing deformation of a banded grain so as to minimise its plastic power of deformation, 2) the immobility of DBBs relative to DBs, and 3) the rotation of DBBs with the shape of the grain, can only be tested by comparing the

predictions of this theory with experiment. However, the more fundamental assumption of the theory that large misorientations develop across favourably oriented DBBs with slight misorientations is based on the experimental observations of Cizek et al. (1995), and Hughes and Hansen (1997).

4 Results and discussion

We use the present theory to simulate plastic deformation under uniaxial tension, uniaxial compression, and plane strain rolling, of a 200 grain aggregate, whose orientations are initially random and uniformly distributed over all possible orientations. Taylor polycrystal approximation is assumed, viz., the macroscopically imposed deformation is experienced by each grain. This ensures compatibility across grain boundaries, but in general, results in the violation of equilibrium across them.

Our polycrystal plasticity code implements an incremental formulation of rigid-plastic crystal plasticity obeying the viscoplastic constitutive equation, Eq. (9). The entire deformation is divided into small steps of strain increments, at each of which the shear rates $\dot{\gamma}^s$ of each slip system are calculated according to Eq. (9), and the orientation of each grain or band, and hardness of slip systems within each grain or band is updated. These updates are discussed by Kocks et al. (1998, Chap. 8). The Voce hardening law as extended by Tomé et al. (1984) to account for non-saturation of flow stresses (stage IV hardening) is assumed with no latent hardening of slip systems due to the activity of other slip systems. If τ_s^c is the critical resolved shear stress in slip system s, and the accumulated strain in that system is Γ, the hardening law relates them as

$$\tau_s^c(\Gamma) = \tau_0 + (\tau_1 + \theta_1\Gamma)\left[1 - \exp\left(-\theta_0\Gamma/\tau_1\right)\right]. \tag{33}$$

τ_0, τ_1, θ_0, and θ_1 are material parameters. At each step, the banding condition discussed in

Section 3.2 is checked, if the grain is not already banded. If it is banded, it is not allowed to band further. The procedure of Section 3.3 is used to compute the stress and slip rates of the S slip systems in each band.

We will now apply the present theory of inhomogeneous grain deformation to F.C.C. aluminium and B.C.C. α-iron subjected to monotonic tension, compression, and plane strain rolling deformations. Aluminium grains are assumed to deform solely by $\langle 110\rangle(111)$ slip and α-iron grains solely by $\langle 111\rangle(110)$ slip. In mild steel, Duggan et al. (1998) find it important to consider both $\langle 111\rangle(110)$ and $\langle 112\rangle(111)$ slip, and to adjust the critical resolved shear stress ratio of the two systems appropriately to capture the cold rolling texture. However, for reasons of simplicity in interpreting the results of the model, especially in view of the difficulty of disentangling the contributions to texture evolution of deformation banding and enhanced latent hardening in a $\langle 111\rangle(110)+\langle 112\rangle(111)$ slipping grain, we limit our α-iron model grains to $\langle 111\rangle(110)$ slip only. We will see below (figure 7) that this assumption notwithstanding, the present model succeeds in capturing banding behavior of α-iron. Also, in comparing B.C.C. and F.C.C. banding behaviour, ideally data at the same homologous temperature will be considered. However, only room temperature experimental data is presently available for both metals, and this will be used.

In discussing tension and compression below, the sample coordinate system is such that its '1' axis is along the tensile (TA) or compressive axes (CA). In discussing rolling, the sample '1'-axis is along the rolling direction (RD), the '2'-axis along the transverse direction (TD) and the '3'-axis along the normal direction (ND).

Experimental tensile stress-strain curves for the two metals under consideration, large grained (400 μm average grain diameter) aluminium and α-iron, have been reported by Sil and Varma (1993) and Tjerkstra (1961), respectively. In the single crystal aluminium specimen of Basson and Driver (2000), typical DB width is of the order of 40 μm, so one may expect about 10 DB to form in the grains studied by Sil and Varma, in a way reasonably undisturbed by flow field inhomogeneities due to grain-grain interactions, which predominate

in fine grained polycrystals (Dawson et al. 2002). Also, only large grains can accommodate large dislocation structures, the importance of which was discussed in Section 1 in connection with Winther's observation.

[Figure 4 about here.]

[Table 1 about here.]

The experimental stress-strain curves for aluminium and α-iron allow us to the calibrate the deformation banding model. Table 1 lists the parameters thus fit. The values of k_ω and r were approximated for aluminium from the data of Hughes et al. (1997), and lacking such information for iron, the same values are used. c was discussed below Eq. (21). The values of κ_b and κ_c/D_0^2 were chosen small enough that banding will be possible, and with such a ratio that Eq. (30) will result in about 10 bands in banding grains. Furthermore, we require that κ_c/D_0^2 be such that Eq. (26) yields a reasonable value for δ_c: with $N = 10$, $D = 400 \cdot 10^{-6}$ m, the present value of $\kappa_c/D_0^2 = 1000$ m^{-1} results in $\delta_c = 1.6$ μm, which seems plausible. These estimates can be expected to be correct only in their orders of magnitude, and not in their numerical value. Lacking any motivation for distinction in their values between aluminium and iron, we take both the same. Keeping the above deformation banding parameters fixed, the hardening parameters of Eq. (33) were adjusted until good agreement was obtained between the calculated and experimental curves.

The exact numerical value of these parameters is unimportant. It seldom happens that the banding condition fails because $\dot{W}_H - \dot{W}_i^* < \dot{W}_b + \dot{W}_c$ in Eq. (1). In fact, given our parameter set, the right side of this inequality hardly ever exceeds 10% of the left side, whenever the left side is positive. In this observation, the present model agrees with Lee et al. (1995), who suggest simply taking $\dot{W}_b + \dot{W}_c = 0.05\dot{W}_i$ in Eq. (1). A far more common reason that a simulation grain does not band is that $\min \dot{W}_i$ is achieved at $w \leq c$, or $w \geq 1-c$ (see text below Eq. (21)), or $N = 0$ (see text below Eq. (30)).

Figure 4 shows the good fit between the stress-strain curves calculated using these parameters and the experimental data in uniaxial tension. The experimental data go only up to $\epsilon_{11} = 0.25$; the calculations have been carried out to twice that strain. Also shown in this figure for comparison, are the calculated stress-strain curves in tension obtained by suppressing banding. Note that the polycrystal material that allows for banding is the softer one in both metals, as expected from the energetic basis of computing the deformation of banded grains. It is reassuring that the difference between the banded and homogeneous response of a polycrystal is not very big; classical models are adequate to predict mechanical response when the grain substructure is not of interest.

However, allowing for banding makes far less difference during tension of F.C.C. aluminium (the flow stress gap between the banding and homogeneous polycrystals is only 0.65 MPa, or 1% at $\epsilon_{11} = 0.5$), than of B.C.C. iron (the gap is 12.2 MPa, or 4%). Figure 4 also shows the calculated compression stress-strain curve for polycrystals of both metals doing both banded and homogeneous deformation. In compression, the importance of microstructure reverses between aluminium (the gap is 2.29 MPa, or 6% at $\epsilon_{11} = 0.5$) and iron (the gap is 3.06 MPa or 1.5% at $\epsilon_{11} = 0.5$). Since in compression and rolling (and *not* in tension), as the grains become flatter with deformation, relaxed constraints (RC), rather than full constraints (FC) may be a better approximation of the deformation imposed on a grain, stress-strain curves assuming RC and allowing for banding are also shown. As can be seen, the RC prediction is softer than the FC prediction. Also, the RC curve appears poised to intersect the FC curve in the case of aluminium, but not in the case of iron.

[Figure 5 about here.]

[Figure 6 about here.]

The reversal in the importance of banding between tension and compression, and the contrasting behaviour of the difference between FC and RC curves can be explained by studying the predicted microstructure in each metal. Figure 5 shows the calculated misorientation

distribution across DBBs at $|\epsilon_{11}| = 0.5$ in tension, compression and rolling. As seen, the frequency of grains with large misorientations is larger in compression than in tension in F.C.C. aluminium and vice versa in B.C.C. steel. Thus, banded grains deform more similar to homogeneous ones in tension in F.C.C. aluminium than during compression, and vice versa in B.C.C. iron. This explains the smaller influence of banding on flow response during tension than compression in aluminium, and the opposite situation in iron.

Figure 6 shows the progress of banding in the polycrystal with deformation. The number of grains banding during RC deformation (both in compression and rolling) is smaller than that in FC deformation. This seems reasonable, for if a grain is able to relax its stresses by means of RC, it should have a smaller tendency to band, as banding is simply another means of relaxing components of the stress. The tendency to band under RC is however greater in iron than in aluminium. This suggests a reason why the FC and RC compression flow stress curves in aluminium tend toward each other, while those of iron do not (figure 4). While the RC aluminium curve allowing for banding is initially softer than the FC curve, too few grains band in the RC polycrystal, which results in its getting harder relative to the FC polycrystal after further deformation. Although in iron too, the number of bands formed by the RC polycrystal in compression is fewer than in the FC polycrystal, this number is larger than in aluminium, and seems to lead to an increasing divergence between the RC and FC iron compression curves in figure 4.

[Figure 7 about here.]

In figure 7, we have reproduced the experimental observations of Barrett and Levenson (1940) in pure aluminium, and of Barrett (1939) in mild steel depleted of carbon. It shows the initial orientation of grains that did or did not develop bands after nominally uniaxial compression: compression between lubricated plates to $\epsilon_{11} = -1.89$, followed by 'compression rolling' to varying further reductions in the case of aluminium. In the case of mild steel, Barrett's experimental results were obtained on single crystals.

The mechanical response of Barrett's and Barrett and Levenson's materials was not published. As an approximation, therefore, we assume that their material also approximately flows as the experimental data in figure 4. These data however only go up to $\epsilon_{11} = 0.25$, giving little indication of the flow response in stage IV, which will be of importance at the extremely high deformations imposed experimentally by Barrett and Levenson. Furthermore, the experimental data presented for iron corresponds to single crystals compressed to a range of reductions. Thus, at best, one can expect to qualitatively compare the predictions of the present theory with this experimental data. We therefore simulate FC and RC compression only to $\epsilon_{11} = -0.5$, and plot the initial orientation of each grain in the inverse pole figures of figure 7 for aluminium and iron, with a symbol that denotes the misorientation across the DBB in each banded grain.

In the case of aluminium, both FC and RC simulations of deformation suggest that the grains that band have initial orientations close to the [111] corner. These bands must therefore be forming early in the deformation, since orientations near [111] move toward [110] quite rapidly (see also figure 12). The FC calculation predicts more banded grains than RC, spilling into the main part of the triangle. Some banding also takes place near the [100] corner, and none at all near the [110] corner of the pole figure triangle. Barrett and Levenson also observe many banded grains in the main part of the triangle, and near the [100] corner, but none near [110]. The main discrepancy between the FC predictions and the experimental observation lies at the [111] corner. Here however, Barrett and Levenson have but one data point, and three of the nearest four data points show banding grains. For this reason, we are not certain that there actually is a discrepancy between experiment and calculation here too.

In the case of iron, the FC and RC computations show qualitative distinctions among themselves. FC bands are concentrated near the [110] corner, while RC bands form near the [110] – [111] and [111] – [100] lines. Realizing that the actual constraint experienced by the grain lies somewhere in between the extremes defined by FC, and RC, one can qualitatively

view the actual banding pattern in the polycrystal as lying in between the two predictions shown. The experimental observation of Barrett qualitatively agrees with this. It shows no banding near the [100] corner, although again the [111] corner is uncertain. Banding does occur at the [110] corner and spills into the main part of the triangle.

[Figure 8 about here.]

[Figure 9 about here.]

[Figure 10 about here.]

Figure 8 represents the orientation of DBB normals on pole figures after deformation to strain $|\epsilon_{11}| = 0.5$ in tension, compression, and rolling. As is seen, there is a clear tendency of DBB normals away from the loading axis in tension, and toward the loading axis in compression both in aluminium and α-iron. This is a consequence of the assumption that DBB orientation follows the deformation of the grain as a whole (Eq. (32)). The shape change and normal $\mathbf{n}_1$ reorientation is depicted schematically in figure 9. The exceptionally oriented DBB, labelled $\mathbf{n}_2$ in figure 9, with normals parallel to the loading axis in tension, and perpendicular to it in compression, form close to that orientation at the instant of banding, and are not reoriented significantly with grain deformation.

The orientations of the DBB normals after compression, calculated using RC appear qualitatively different in F.C.C. aluminium and B.C.C. iron than those calculated using FC. This is because aluminium grains that would have banded with normals not perpendicular to the compression axis under FC, do not band at all under RC. This suggests that RC deformation suffices to adequately relax the stress in these grains, thereby obviating deformation banding. However, in the case of iron, it is the complementary set of grains, those with normals not perpendicular to the compression axis, that do band.

After rolling, in both aluminium and iron, there is a definite tendency of the DBB normal orientation away from the rolling direction, in agreement with the experimental observations

of Lee and Duggan (1993). In FC rolled aluminium, the normal is approximately uniformly distributed perpendicular to the RD; however, there is clear propensity for the normal to be parallel to the ND in the case of rolled iron. These tendencies persist in RC rolled aluminium and iron, although fewer grains band under RC.

We next turn toward misorientation axes across DBB shown in figure 10. In FC tension and compression, both in aluminium and iron, a clear tendency of the misorientation axis toward the loading axis can be seen. This tendency is not so clear in RC compression, but it appears plausible that with continued deformation, the misorientation axes will rotate parallel to the loading axis even in this case. Taken together with the previous observation of DBB normal orientations, this implies that the tensile DBB in both metals have a predominantly 'tilt' character, while the compressive DBB have a predominantly 'twist' character.

In both aluminium and iron, subjected to either FC or RC plane strain rolling, there is a pronounced tendency of the DBB misorientation axis away from the transverse direction (TD). This conflicts with the experimental observations of Liu and Hansen (1998), and Liu et al. (2000) who experimentally studied rolling of unstable cube oriented ((001)/[100]) single aluminium crystals and found a clear preference for rotation about the TD of deformation bands. Li et al. (2004) found the same in unstable (001)/[110] Al-1%Mn. During channel-die compression, Driver and co-workers (Akef and Driver 1991, Basson and Driver 2000) also observed the same.

[Figure 11 about here.]

As discussed by Liu et al. (2000), rotation about TD under plane strain deformation will increase the power of deformation, and explains why the present model does not predict this rotation. Liu et al also hypothesised that in rolling experiments, a shear component due to geometric and frictional effects previously studied by Lee and Duggan (1991) may be causing the rotations about TD. Lee and Duggan (1991) have quantified the requisite magnitude of the shear component to be about 1.5 times the rolling strain to yield the

correct textures. Figure 11 shows the effect of this shear component on the orientation of the misorientation axis in (001)/[100] and (001)/[110] aluminium crystals at $\epsilon_{11} = 0.5$. $\mathbf{L}$ here denotes the velocity gradient, and its matrix representation given in the figure corresponds to the coordinate axes described on p. 23. Clearly, the misorientation axis of the cube oriented crystal, which under plane strain is nearly parallel to the RD is redirected along TD in the presence of the shear component. The reorientation due to shear of the (001)/[110] orientation is also very nearly parallel to the TD. It should also be mentioned that although these special orientations show rotation of their bands about the TD, the majority of the (initially randomly oriented) grains continue to rotate about an axis nearly perpendicular to the TD regardless of the imposed shear component $L_{13} = -1.5$; the misorientation axis pole figure under this condition of 200 aluminium grains looks similar to that of the iron polycrystal under FC rolling in figure 10.

Although the frictional and geometric effects considered by Lee and Duggan do not apply to the channel-die experiments of Driver and co-workers, we suspect that here too, the observed misorientation axis is due to an uncharacterised experimental condition. It is known (Humphreys and Ardakani 1994) that slight differences in the material constitution or initial orientation of the crystals can cause qualitative differences in the banding behaviour.

[Figure 12 about here.]

[Figure 13 about here.]

Figures 12 and 13 show the calculated texture developed during tension, compression, and rolling in aluminium and iron respectively under three different deformation assumptions: FC and RC, with and without allowing grain banding, As is to be expected, the RC and FC pole figures are qualitatively different. However, banding does not introduce any noticeable qualitative change in the pole figures. It is however seen by comparing intensities that banding does make the pole figures less sharp. Another point to notice is that there is

no systematic separation between heavy and light bands during deformation: both move statistically similarly through orientation space.

[Table 2 about here.]

Deformation banding lowers the number of active slip systems in banded grains. To quantify the reduction, following Kocks et al. (1998, Chap. 11), we define the average number of active systems per grain, $\langle n_{\text{active}} \rangle$ as

$$\langle n_{\text{active}} \rangle = \frac{\sum_g n_{\text{active},g} V_g}{\sum_g V_g} \tag{34}$$

where the summations run over all the bands and grains in the polycrystal. The volume fraction of the band or grain relative to the polycrystal is denoted by V_g, and its total slip rate, $\dot{\Gamma}_g = \sum_s |\dot{\gamma}^s(g)|$. $n_{\text{active},g}$ is the number of *active* slip systems in grain or band g, where a slip system is taken to be active if its slip rate exceeds 5% of the maximum slip rate in that grain or band. Table 2 lists $\langle n_{\text{active}} \rangle$ under various deformation conditions applied to both aluminium and iron under both FC and RC constraints. It is plainly seen that the reduction in $\langle n_{\text{active}} \rangle$ is larger under FC than under RC for both metals, both because fewer grains band under RC, and because relaxation of constraints acts as an alternative mechanism to lower the plastic power of deformation. Thus, on the basis of its physical hypotheses, the present theory lowers $\langle n_{\text{active}} \rangle$, and hence latent hardening.

5 Conclusions and future work

A theory of inhomogeneous grain deformation has been developed, and used to model deformation banding. According to this theory, deformation bands are initiated at a favourably oriented IDB and develop so as to minimise the plastic power of grain deformation. The banding criterion is dominated by minimisation of plastic deformation power, with the accommodation power at band and grain boundaries, playing a far lesser role. The model

predicts a number of microstructural features of grains in plastically deforming aluminium and α-iron. Comparison with experimental data has been attempted, where such data is available. Experimentally, the formation and evolution of deformation bands can be very sensitive to material and experimental conditions; the large variability in the results of nominally identical loading conditions on nominally identical materials (see e.g., Liu and Hansen 1998, Sec. 4(b)), makes quantitative comparisons between theory and experiment difficult. At best therefore, only qualitative comparisons are presently possible. Such comparisons are favourable.

The present theory of deformation banding fundamentally differs from that of Lee and Duggan, and Ortiz and co-workers in that an explicit mechanism is proposed here for the initiation of deformation bands from misorientations seeded by IDBs. The latent hardening assumption is not essential for our grains to band; in fact, the banding decision is an instantaneous one based on the present state of the grain as represented by the critical resolved shear stresses of all its slip systems, average grain orientation, and the imposed loading. The present theory however reduces the number of active slip systems in each band from that in a grain; in this sense, it reduces latent hardening of the grain as a consequence of its physical hypotheses. Also, the deformation banding criterion does not hinge on rate sensitivity of the grain's constitutive law.

Several extensions of the present theory are possible; four of them are as follows. Firstly, the two different constraining schemes investigated in the present work (FC and RC) represent limiting cases of the actual constraint experienced by the grain. The self-consistent scheme (Lebensohn and Tomé 1993) represents a better intermediate approximation of the grain constraints in a polycrystal, and the banding theory, incorporated in the self-consistent framework should give intermediate results. Here we choose not to pursue the self-consistent model to better isolate the effect of deformation and orientation on banding behavior of a grain. The same can be said of latent hardening: introducing it in the present calculations would make it harder to interpret our results. Secondly, the present theory allows at most

one set of parallel bands to form in each grain. In reality, secondary and tertiary bands are observed (Kulkarni et al. 1998), which are still many times as big as the mean free path of individual dislocations. Such banding could be permitted. Thirdly, once banded, grains in the present model deform as a composite grain as described in Section 3.3. In reality though, after a certain deformation, bands 'release' and deform as independent new grains (Duggan and Lee 1996). Such a release condition may be effected when a threshold misorientation is achieved. Finally, we believe the present model can be adapted to simulate martensitic or deformation twinning transformations. Both transformations concentrate shears within bands in grains.

Acknowledgments

This research is funded by DOE, Office of Science, Office of Basic Energy Sciences. We thank Dr. R. J. McCabe for helpful criticism of this manuscript.

A Minimising plastic power of a banded grain

Here we show that to minimise the plastic power of a banded grain

$$\dot{W}_i = w \sum_{s=1}^{S} \tau_s \left| \frac{\boldsymbol{\sigma}^{(1)} : \mathbf{m}^{s,(1)}}{\tau^s} \right|^{n+1} + (1-w) \sum_{s=1}^{S} \tau_s \left| \frac{\boldsymbol{\sigma}^{(2)} : \mathbf{m}^{s,(2)}}{\tau^s} \right|^{n+1}. \tag{35}$$

subject to full constraints Eq. (13),

$$\begin{aligned} 0 = \dot{\epsilon}_j^G &- w \sum_{s=1}^{S} \mathbf{m}_j^{s,(1)} \left| \frac{\boldsymbol{\sigma}^{(1)} : \mathbf{m}^{s,(1)}}{\tau^s} \right|^{n} \operatorname{sign}(\boldsymbol{\sigma}^{(1)} : \mathbf{m}^{s,(1)}) \\ &- (1-w) \sum_{s=1}^{S} \mathbf{m}_j^{s,(2)} \left| \frac{\boldsymbol{\sigma}^{(2)} : \mathbf{m}^{s,(2)}}{\tau^s} \right|^{n} \operatorname{sign}(\boldsymbol{\sigma}^{(2)} : \mathbf{m}^{s,(2)}) \end{aligned} \tag{36}$$

for $j = 1, \ldots, 5$ requires that

$$\boldsymbol{\sigma}^{(1)} = \boldsymbol{\sigma}^{(2)}. \tag{37}$$

If $\lambda_j,\ j=1,\ldots,5$ are Lagrange multipliers, and

$$\begin{aligned}\mathscr{L} &= w\sum_{s=1}^{S}\tau_s\left|\frac{\boldsymbol{\sigma}^{(1)}:\mathbf{m}^{s,(1)}}{\tau^s}\right|^{n+1} + (1-w)\sum_{s=1}^{S}\tau_s\left|\frac{\boldsymbol{\sigma}^{(2)}:\mathbf{m}^{s,(2)}}{\tau^s}\right|^{n+1}\\ &+\lambda_j\left[\dot{\epsilon}_j^G - w\sum_{s=1}^{S}\mathbf{m}_j^{s,(1)}\left|\frac{\boldsymbol{\sigma}^{(1)}:\mathbf{m}^{s,(1)}}{\tau^s}\right|^{n}\operatorname{sign}(\boldsymbol{\sigma}^{(1)}:\mathbf{m}^{s,(1)})\right.\\ &\left.-(1-w)\sum_{s=1}^{S}\mathbf{m}_j^{s,(2)}\left|\frac{\boldsymbol{\sigma}^{(2)}:\mathbf{m}^{s,(2)}}{\tau^s}\right|^{n}\operatorname{sign}(\boldsymbol{\sigma}^{(2)}:\mathbf{m}^{s,(2)})\right],\end{aligned} \tag{38}$$

where summation over the repeated index j is implied, then, the constrained relative extrema of $\dot{W}_i$ are given by

$$\frac{\partial\mathscr{L}}{\partial\sigma_j^{(1)}} = \frac{\partial\mathscr{L}}{\partial\sigma_j^{(2)}} = \frac{\partial\mathscr{L}}{\partial\lambda_j} = 0. \tag{39}$$

Eq. (39) is satisfied if

$$\lambda_j = \frac{n+1}{n}\sigma_j^{(1)} = \frac{n+1}{n}\sigma_j^{(2)}, \qquad j=1,\ldots,5, \tag{40}$$

which implies Eq. (37).

To show that Eq. (37) characterises not only a relative, but also the absolute (global) minimum, all we need show is that the stress-strain rate relation, Eq. (36) can be derived from a potential $F(\boldsymbol{\sigma}^G)$ according to

$$\dot{\boldsymbol{\epsilon}}^G = \frac{\partial F}{\partial\boldsymbol{\sigma}^G}\,(\boldsymbol{\sigma}^G), \tag{41}$$

where $F(\boldsymbol{\sigma}^G)$ is concave to the origin (Hill (1950, Chap. 2)) in stress space.

$$F(\boldsymbol{\sigma}^G) = \frac{w}{n+1}\sum_{s=1}^{S}\tau_s\left|\frac{\boldsymbol{\sigma}^G:\mathbf{m}^{s,(1)}}{\tau^s}\right|^{n+1} + \frac{1-w}{n+1}\sum_{s=1}^{S}\tau_s\left|\frac{\boldsymbol{\sigma}^G:\mathbf{m}^{s,(2)}}{\tau^s}\right|^{n+1} \tag{42}$$

is such a potential.

Similar considerations apply also in the case that the FC constraints, Eq. (36) are replaced

by RC constraints, Eq. (22), provided that $\sigma_3^G = \sigma_5^G = 0$.

B Estimating $\dot{W}_b$ and $\dot{W}_c$

We consider first the power stored in DBBs, $\dot{W}_b$. Given the dislocation density ρ, shear modulus G, Burgers vector magnitude b, and dislocation interaction parameter $0 \leq \alpha \leq 0.5$, the stored energy per unit volume, i.e., the stored energy density, is approximately (Hughes et al. 2003)

$$\alpha \rho G b^2. \tag{43}$$

Now, according to Kröner's formula (Ortiz et al. 2000), the dislocation density tensor $\mathbf{A}$ between two bands that have deformation gradients $\mathbf{F}^{(1)}$, and $\mathbf{F}^{(2)}$, is

$$\mathbf{A} = [\mathbf{F}] \times \mathbf{n}/\delta_{\mathrm{b}}, \tag{44}$$

where $[\mathbf{F}] = \mathbf{F}^{(2)} - \mathbf{F}^{(1)}$ denotes the jump in deformation gradient across an interface of thickness δ_{b} (see figure 2) with normal $\mathbf{n}$. Recalling that (Nye 1953),

$$\mathbf{A} = \sum_{s=1}^{S} \rho^s \boldsymbol{\beta}^s \otimes \boldsymbol{\xi}^s, \tag{45}$$

where ρ^s is the dislocation density with (non-unit) Burgers vector $\boldsymbol{\beta}^s$, $\|\boldsymbol{\beta}^s\| = b$, $\forall s$, and unit line direction vector $\boldsymbol{\xi}^s$. The norm of $\mathbf{A}$, $\|\mathbf{A}\| = \sqrt{\mathbf{A} : \mathbf{A}}$ is therefore of the order $\|\mathbf{A}\| \approx (\sum_s \rho^s) b = \rho b$. Then, the approximate energy stored per unit DBB volume in a grain whose bands have deformation gradients $\mathbf{F}^{(1)}$, and $\mathbf{F}^{(2)}$ is $\alpha G b \|\mathbf{A}\|$. Assuming the grain to be a sphere of diameter D, and assuming that N DBB form in the grain, the volume of DBB per unit grain volume goes as $N D^2 \delta_{\mathrm{b}} / D^3$, so that the stored energy per unit grain volume is given by $\kappa_b N \alpha G b \delta_{\mathrm{b}} \|\mathbf{A}\| / D$, where we have absorbed all the uncertainties of estimation into the parameter κ_b.

We are interested in the stored *power* density at the instant of banding. Thus,

$$\dot{W}_b = \kappa_b \left(\frac{N\alpha Gb}{D} \right) \frac{d\|[\mathbf{F}] \times \mathbf{n}\|}{dt}, \tag{46}$$

which is independent of δ_b. Let $\mathbf{F}_0$ be the deformation gradient of the grain and $\mathbf{L}_0^{(1)}$, and $\mathbf{L}_0^{(2)}$, their respective velocity gradients at the instant of deformation banding. By definition, at the instant of banding, each band of the grain has the same deformation gradient, so that $[\mathbf{F}_0] = \mathbf{0}$ across any plane. Let $\mathbf{F}_t^{(1)}$, and $\mathbf{F}_t^{(2)}$ be the deformation gradient of the bands at time t after their formation. Then, to a good approximation if t is small, according to Eq. (7), $\mathbf{F}_t^{(i)} = \mathbf{F}_0 + t\mathbf{L}_0^{(i)}\mathbf{F}_0$, for $i = 1, 2$. Thus, $[\mathbf{F}_t] = t[\mathbf{L}_0]\mathbf{F}_0$. Rewriting Eq. (46) as

$$\dot{W}_b = \kappa_b \frac{N\alpha Gb}{D} \lim_{t \downarrow 0} \frac{\|[\mathbf{F}_t] \times \mathbf{n}\| - \|[\mathbf{F}_0] \times \mathbf{n}\|}{t}, \tag{47}$$

and applying the preceding conclusions results in

$$\dot{W}_b = \kappa_b \frac{N\alpha Gb}{D} \|[\mathbf{L}_0]\mathbf{F}_0 \times \mathbf{n}\|. \tag{48}$$

We next turn toward estimating $\dot{W}_c$. As already noted, homogeneously deforming grains in a Taylor polycrystal are compatible across the grain boundary. The average deformation gradient of a grain $\mathbf{F}^G$ with two bands whose grain relative volume fractions are w and $1-w$ and whose individual deformation gradients are $\mathbf{F}^{(1)}$, and $\mathbf{F}^{(2)}$, respectively is

$$\mathbf{F}^G = w\mathbf{F}^{(1)} + (1-w)\mathbf{F}^{(2)}. \tag{49}$$

By deforming inhomogeneously, the grain creates incompatibilities at the grain boundary as shown in figure 2, which are to be accommodated through inhomogeneous deformations at the grain boundary through the generation and storage of GND.

To approximate $\dot{W}_c$ in Eq. (1), we use an argument similar to that of Ashby (1970).

Consider the difference in deformation (physically, a void or material interpenetration) that will be created in a band of length equal to the grain diameter D due to its deformation with gradient $\mathbf{F}^{(1)}$ instead of $\mathbf{F}^G$. We may regard $\|\mathbf{F}^{(1)} - \mathbf{F}^G\|D$ as a scalar measure of this deformation difference. To fill this difference will take $\|\mathbf{F}^{(1)} - \mathbf{F}^G\|D/b$ GND, where b is the magnitude of the GND Burgers vector. If there are $N+1$ DB in the grain, half $((N+1)/2)$ of which have volume fraction w, and the other half have volume fraction $1-w$, the grain boundary area corresponding to the first type of band goes as $2D^2w/(N+1)$. So, the dislocation density ρ needed to accommodate the first type of band goes as $(N+1)\|\mathbf{F}^{(1)} - \mathbf{F}^G\|/(2Dbw)$, and according to Eq. (43), the stored energy goes as $\alpha Gb(N+1)\|\mathbf{F}^{(1)} - \mathbf{F}^G\|/(2Dw)$. As shown in figure 2, let δ_c be the thickness of the accommodation layer at the grain boundary, where the GND form by inhomogeneous deformation. Then, the volume fraction of the accommodation layer in the first type of bands is $D^2\delta_c w/D^3 = w\delta_c/D$, so that the stored energy density in the first type of bands (with deformation gradient $\mathbf{F}^{(1)}$) is $(\alpha Gb\delta_c(N+1)/(2D^2))\|\mathbf{F}^{(1)} - \mathbf{F}^G\|$, which is independent of w. Similarly, the stored energy density in the second type of bands (with deformation gradient $\mathbf{F}^{(2)}$) is $(\alpha Gb\delta_c(N+1)/(2D^2))\|\mathbf{F}^{(2)} - \mathbf{F}^G\|$.

Observing from Eq. (49) that $\mathbf{F}^{(1)} - \mathbf{F}^G = (1-w)[\mathbf{F}]$, and $\mathbf{F}^{(2)} - \mathbf{F}^G = w[\mathbf{F}]$, and summing the two stored energy contributions above, we have

$$W_c = \frac{\alpha Gb(N+1)\delta_c}{2D^2}\|[\mathbf{F}]\|. \tag{50}$$

Thus,

$$\dot{W}_c = \frac{\alpha Gb(N+1)\delta_c}{2D^2}\lim_{t\downarrow 0}\frac{\|[\mathbf{F}_t]\| - \|[\mathbf{F}_0]\|}{t}. \tag{51}$$

Using arguments similar to those preceding Eq. (48), and letting $N+1 \approx N$, in view of the considerable assumptions made, we finally have

$$\dot{W}_c = \frac{N}{2}\frac{\alpha Gb\delta_c}{D^2}\|[\mathbf{L}_0]\mathbf{F}_0\|. \tag{52}$$

References

Ahlborn, H. 1966, Recrystallization, grain growth, and textures, (Metals Park, Ohio: ASM), pp. 374–381.

Ahlborn, H. 1966b, *Z. Metallkd.* **57**, 877.

Akef, A. and Driver, J. H. 1991, *Mat. Sci. Eng. A* **A132**, 245.

Argon, A. S. 2002, *Scripta mater.* **47**, 683.

Asaro, R. J. and Needleman, A. 1985, *Acta metall.* **33**, 923.

Ashby, M. F. 1970, *Phil. Mag.* **21**, 399.

Barrett, C. S. 1939, *Trans. AIME* **135**, 296.

Barrett, C. S. and Levenson, L. H. 1940, *Trans. AIME* **137**, 112.

Basson, F. and Driver, J. H. 2000, *Acta mater.* **48**, 2101.

Bay, B., Hansen, N., Hughes, D. A. and Kuhlmann-Wilsdorf, D. 1992, *Acta metall. mater.* **40**, 205.

Bishop, J. F. W. and Hill, R. 1951*a*, *Phil. Mag.* **42**, 1298.

Bishop, J. F. W. and Hill, R. 1951*b*, *Phil. Mag.* **42**, 414.

Canova, G. R., Fressengeas, C., Molinari, A. and Kocks, U. F. 1988, *Acta Metall.* **38**, 1961.

Chin, G. Y. and Mammel, W. L. 1969, *Trans. AIME* **245**, 1211.

Chin, G. Y. and Wonsiewicz, B. C. 1969, *Trans. AIME* **245**, 871.

Christoffersen, H. and Leffers, T. 1998, *Acta mater.* **46**, 4093.

Cizek, P., Parker, B. A. and Wynne, B. J. 1995, *Scripta metall.* **32**, 319.

Dawson, P. R., Mika, D. P. and Barton, N. R. 2002, *Scripta mater.* **47**, 713.

Dillamore, I. L. and Katoh, H. 1974, *Metal Sci.* **8**, 21.

Duggan, B. J. and Lee, C. S. 1996, Proc. Eleventh Int. Conf. Text. Mat. (ICOTOM 11), edited by Z. Liang, L. Zuo and Y. Chu, (Xian, China: International Academic Publishers).

Duggan, B. J., Liu, G. L. and Zhang, L. X. 1998, *Mater. Sci. Forum* **273–275**, 291.

Gurtin, M. E. 1981, *An introduction to continuum mechanics*, (New York: Academic Press).

Hansen, N. and Jensen, D. J. 1999, *Phil. Trans. R. Soc. Lond. A* **357**, 1447.

Hill, R. 1950, *The mathematical theory of plasticity* (Oxford: Clarendon Press).

Hill, R. 1961, 'Progress in Solid Mechanics', Vol. 2 edited by I. N. Sneddon and R. Hill, (New York: Interscience Publishers) chapter 6.

Hill, R. 1967, *J, Mech. Phys. Solids* **15**, 79.

Hosford, W. F. 1993, *The mechanics of crystals and textured polycrystals* (New York: Oxford University Press)

Huang, X. 1998, *Scripta mater.* **38**, 1697.

Huang, X. and Hansen, N. 1997, *Scripta Mater* **37**, 1.

Hughes, D. A. and Hansen, N. 1993, *Met. Trans.* **24A**, 2021.

Hughes, D. A. and Hansen, N. 1997, *Acta mater.* **45**, 3871.

Hughes, D. A., Hansen, N. and Bammann, D. J. 2003, *Scripta Mater.* **48**, 147.

Hughes, D. A., Liu, Q., Chrzan, D. C. and Hansen, N. 1997, *Acta mater.* **45**, 105.

Humphreys, F. J. and Ardakani, M. G. 1994, *Acta metall. mater.* **42**, 749.

Hutchinson, J. W. 1976, *Proc. R. Soc. Lond. A.* **348**, 101.

Kocks, U. F., Tomé, C. N. and Wenk, H. R. 1998, *Texture and Anisotropy*(Cambridge: Cambridge University Press).

Kuhlmann-Wilsdorf, D. 1999*a*, *Acta mater.* **47**, 1697.

Kuhlmann-Wilsdorf, D. 1999*b*, *Phil. Mag. A.* **79**, 955.

Kulkarni, S. S., Jr, E. A. S. and Kuhlmann-Wilsdorf, D. 1998, *Acta mater.* **46**, 5283.

Lebensohn, R. E. and Tomé, C. N. 1993, *Acta metall. mater* **41**, 2611.

Lee, C. S. and Duggan, B. J. 1991, *Met. Trans. A* **22A**, 2637.

Lee, C. S. and Duggan, B. J. 1993, *Acta metall. mater.* **41**, 2691.

Lee, C. S., Duggan, B. J. and Smallman, R. E. 1993, *Acta metall. mater.* **41**, 2265.

Lee, C. S., Smallman, R. E. and Duggan, B. J. 1995, *Scripta metall. mater.* **33**, 727.

Li, Z. J., Godfrey, A. and Liu, Q. 2004, *Acta mater.* **52**, 149.

Liu, G. and Duggan, B. J. 2001, *Metall. Mater. Trans. A* **32A**, 125.

Liu, Q. and Hansen, N. 1998, *Proc. R. Soc. Lond. A* **454**, 2555.

Liu, Q., Huang, X., Lloyd, D. J. and Hansen, N. 2002, *Acta mater.* **50**, 3789.

Liu, Q., Wert, J. and Hansen, N. 2000, *Acta mater.* **48**, 4267.

Mahesh, S., Tomé, C. N., McCabe, R. J., Kaschner, G., Beyerlein, I. J., and Misra, A. 2004, Submitted to *Metall. mater. trans.*.

Maurice, C. and Driver, J. H. 1993, *Acta metall. mater.* **41**, 1653.

Meyers, M. A. and Ashworth, E. 1982, *Phil. Mag. A* **46**, 737.

Nye, J. F. 1953, *Acta metall.* **1**, 153.

Ortiz, M. and Repetto, E. A. 1999, *J. Mech. Phys Solids* **47**, 397.

Ortiz, M., Repetto, E. A. and Stainier, L. 2000, *J. Mech. Phys. Solids* **48**, 2077.

Peeters, B., Seefeldt, M., Teodosiu, C., Kalidindi, S. R., Houtte, P. V. and Aernoudt, E. 2001, *Acta Mater.* **49**, 1607.

Read, W. T. and Shockley, W. 1950, *Phys. Rev.* **78**, 275.

Sil, D. and Varma, S. K. 1993, *Met. Trans. A* **24A**, 1153.

Spellucci, P. 1998, *Math. Prog.* **82**, 413. FORTRAN code `donlp2`: do nonlinear programming, obtainable via anonymous ftp from netlib.org as netlib/opt/donlp2.

Tjerkstra, H. H. 1961, *Acta metall.* **9**, 259.

Tomé, C., Canova, G. R., Kocks, U. F., Christodoulou, N. and Jonas, J. J. 1984, *Acta metall.* **32**, 1637.

Tse, Y. Y., Liu, G. L. and Duggan, B. J. 2000, *Scripta mater.* **42**, 25.

Wert, J. A. 2002, *Acta mater.* **50**, 3125.

Wert, J. A. and Huang, X. 2003, *Phil. Mag.* **83**, 969.

Winther, G. 2003, *Acta mater.* **51**, 417.

Winther, G., Huang, X. and Hansen, N. 2000, *Acta mater.* **48**, 2187.

Winther, G., Jensen, D. J. and Hansen, N. 1997, *Acta mater.* **45**, 5059.

List of Figures

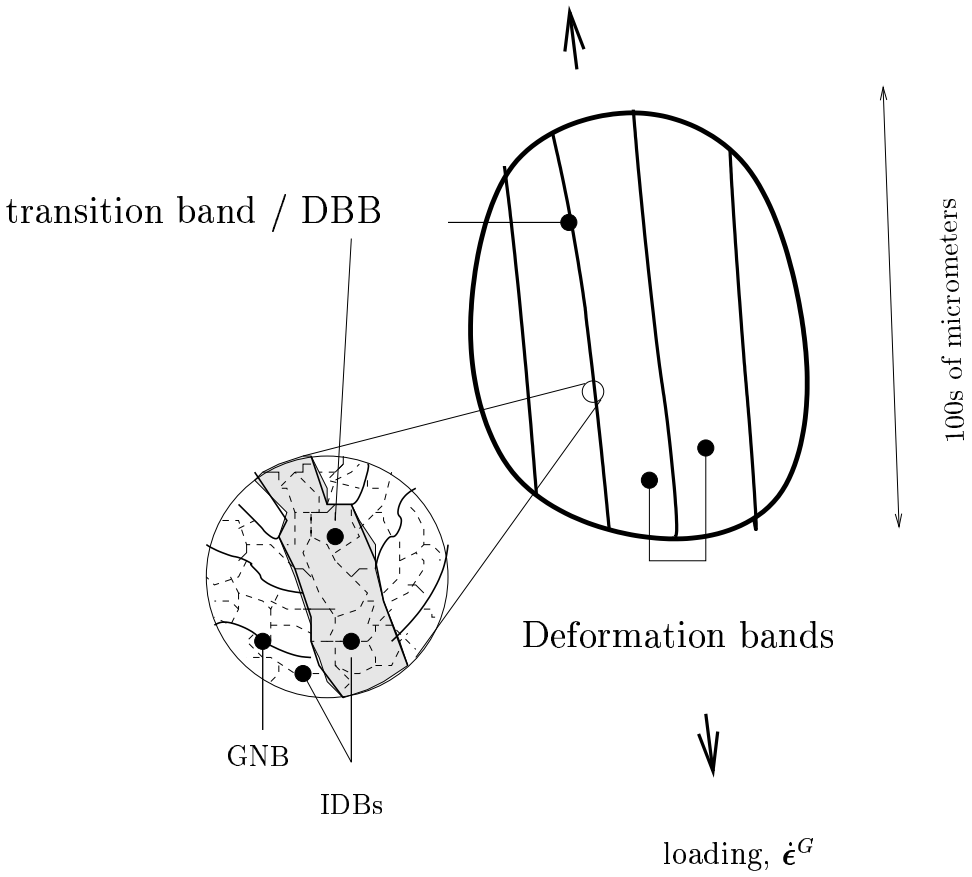

Figure 1: Schematic of the dislocation substructure within a moderate or large-sized grain, showing deformation bands (see Fig. 8 in Kulkarni et al (1998) for a micrograph), and an enlarged view of the substructure near a deformation band boundary, drawn here as a transition band (also see Fig. 19 in Liu and Hansen (1998)). The substructure shown is characteristic of small to moderate deformations ($\lesssim 30\%$ von Mises strain for Al) with a cell and cell-block structure. IDBs enclosing cells are shown as dashed lines, and GNBs enclosing cell blocks as solid lines. The transition band is shown shaded in the enlarged view, and is subdivided largely by dislocation cells. On the other hand, the deformation bands are shown divided by both cells and cell blocks in keeping with the observations of Liu and Hansen (1998).

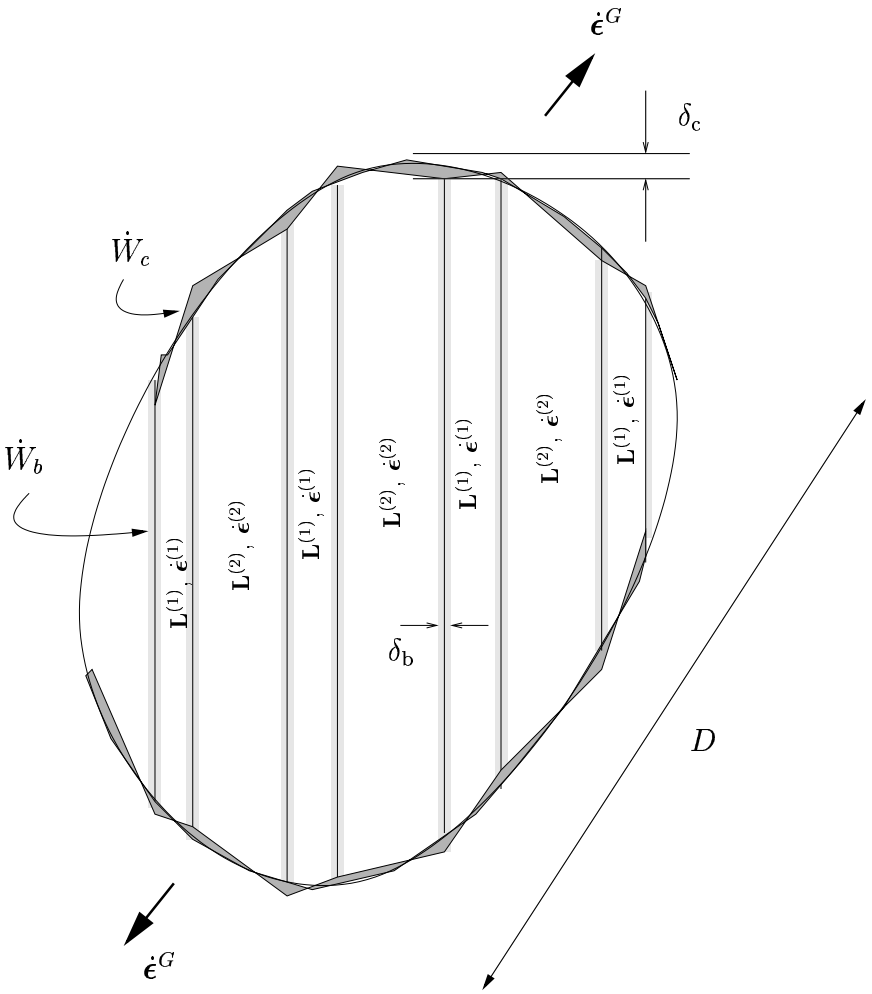

Figure 2: An accommodation band (shown shaded) is typically needed for strain compatibility across grain boundaries and between bands in banded grains, wherein power $\dot{W}_c$ and $\dot{W}_b$, respectively are stored. As shown, the grain has $N = 8$ DBB and $N + 1 = 9$ DB. The DB may have differing volume fractions.

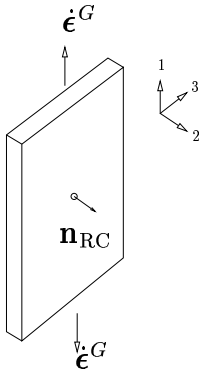

Figure 3: Relaxed constraints are more appropriate to model flat grain deformation than full constraints.

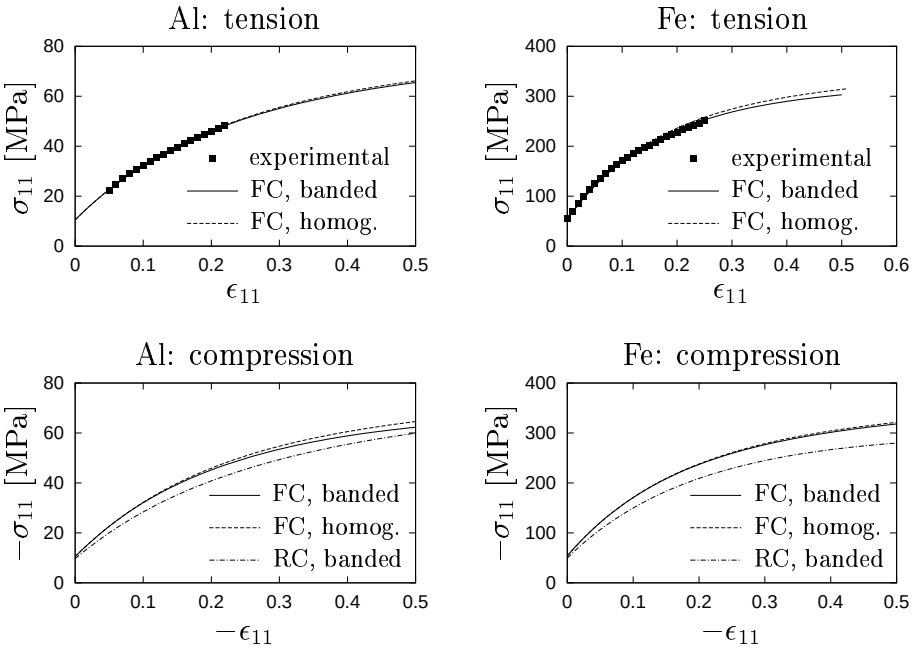

Figure 4: Row 1: Fits of the experimental tensile curve for aluminium and α-iron to the calculated curves assuming deformation banding obtained using the parameters in table 1. Also shown are the curves obtained using these parameters, while suppressing deformation banding. Row 2: Calculated stress-strain curve under compression in both metals using the same parameters.

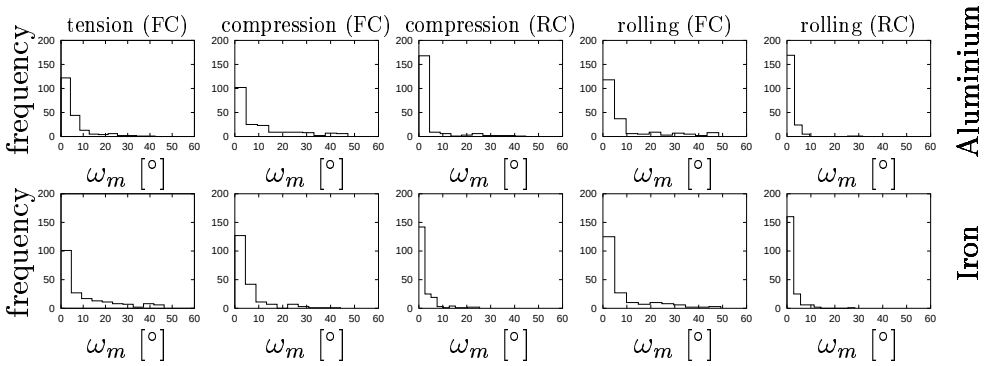

Figure 5: Histograms of the distribution of the computed misorientation between deformation bands at $|\epsilon_{11}| = 0.5$, after tension, compression and rolling under FC and RC constraint conditions. The first row is for aluminium, and the second for α-iron. Both the aluminium and α-iron model polycrystals consist of 200 grains.

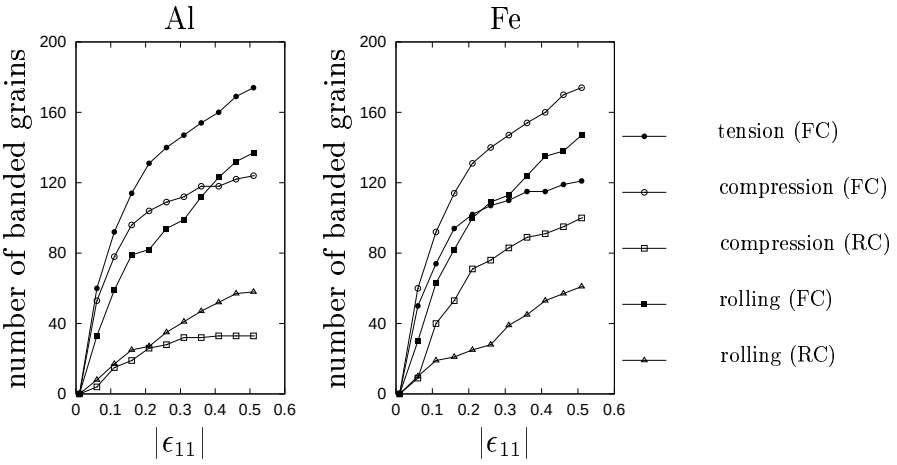

Figure 6: Progress of banding during simulated deformation. Both the aluminium and α-iron model polycrystals consist of 200 grains.

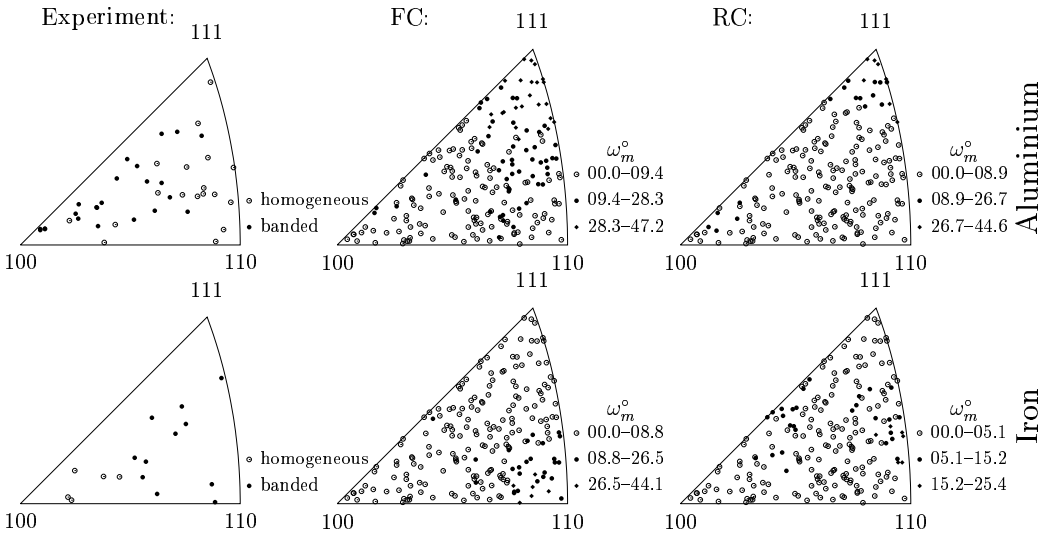

Figure 7: Dependence of misorientation after compression to $\epsilon_{11} = -0.5$ on initial grain orientation. Dots indicate initial (before compression) grain orientation, and the dot shape indicates its misorientation after compression. The rows correspond to aluminium and iron, respectively. First column: inverse compression pole figures experimentally observed by Barrett and Levenson (aluminium), and Barrett (iron). Open symbols denote poles with small misorientation and solid symbols, poles with large misorientations. Second column: calculated inverse pole figure assuming FC. Third column: calculated inverse pole figure assuming RC. Open symbols in columns 2 and 3 denote calculated poles with no or small misorientation (less than 20% of the maximum observed misorientation); solid symbols denote the rest of the poles.

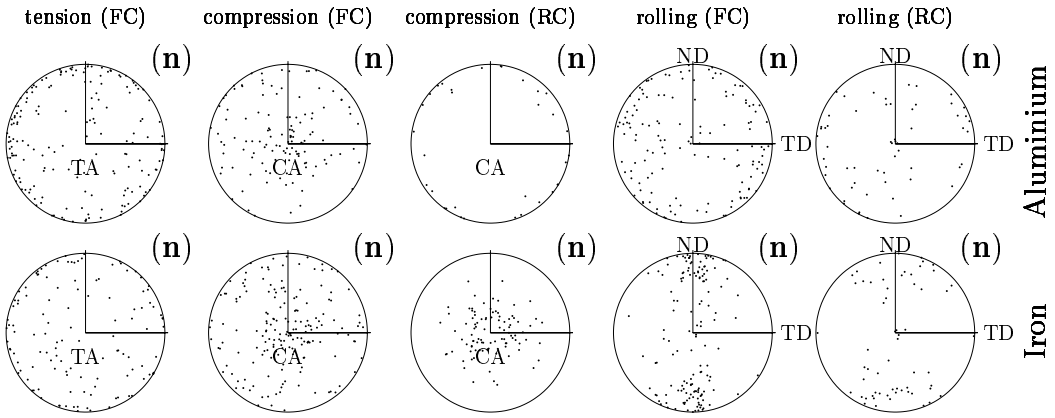

Figure 8: Calculated pole figures (equal area projection, no symmetrisation applied) of the orientation of DBB normals $\mathbf{n}$ after $|\epsilon_{11}| = 0.5$ deformation in tension (only FC), compression and rolling (both FC and RC calculations). TA denotes the tensile axis, CA the compression axis, RD the rolling direction, TD the transverse direction and ND the normal direction. Only grains that band are represented by dots in this figure.

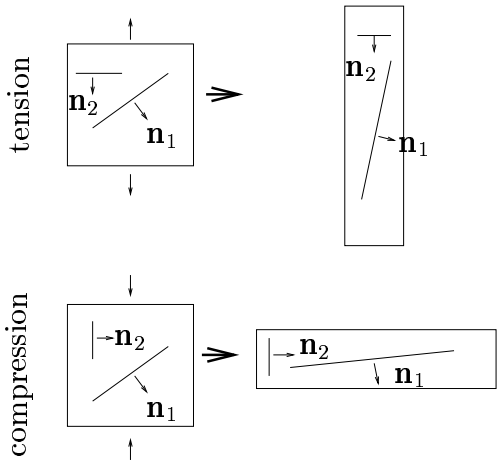

Figure 9: Schematic diagram to explain the observed orientation of DBB normals $\mathbf{n}$.

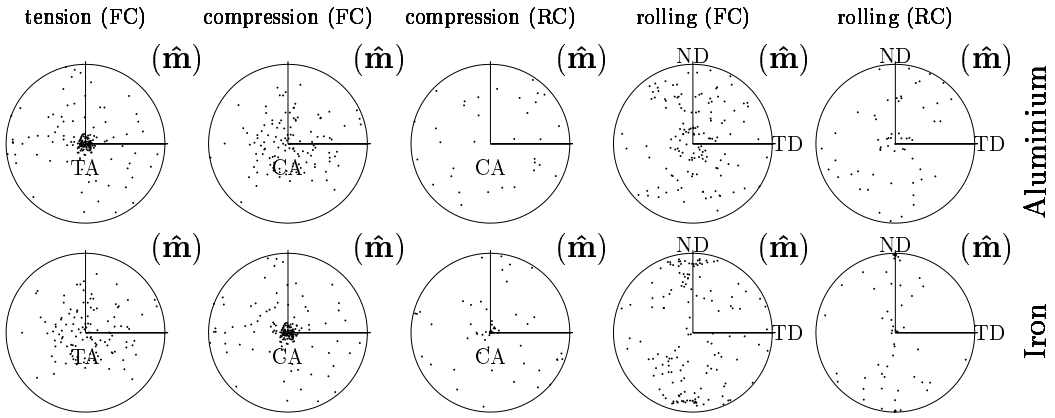

Figure 10: Calculated pole figures (equal area projection) of the orientation of DBB misorientation axes $\hat{\mathbf{m}}$ after $|\epsilon_{11}| = 0.5$ deformation in tension (only FC), compression and rolling (both FC and RC calculations). TA denotes the tensile axis, CA the compression axis, RD the rolling direction, TD the transverse direction and ND the normal direction. Only grains that band are represented by dots in this figure.

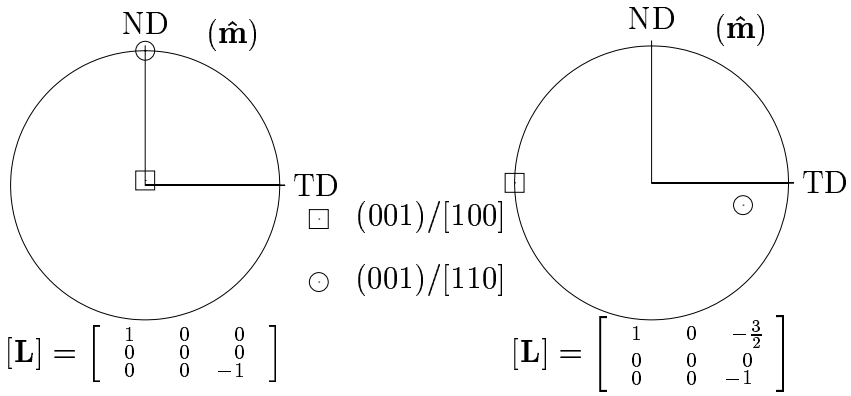

Figure 11: Computed reorientation of the misorientation axis in initially cube oriented (001)/[100] and (001)/[110] oriented single crystals without, and with the shear caused by geometry and friction effects during rolling. Experimentally, the misorientation axis is known to be parallel to TD for these orientations.

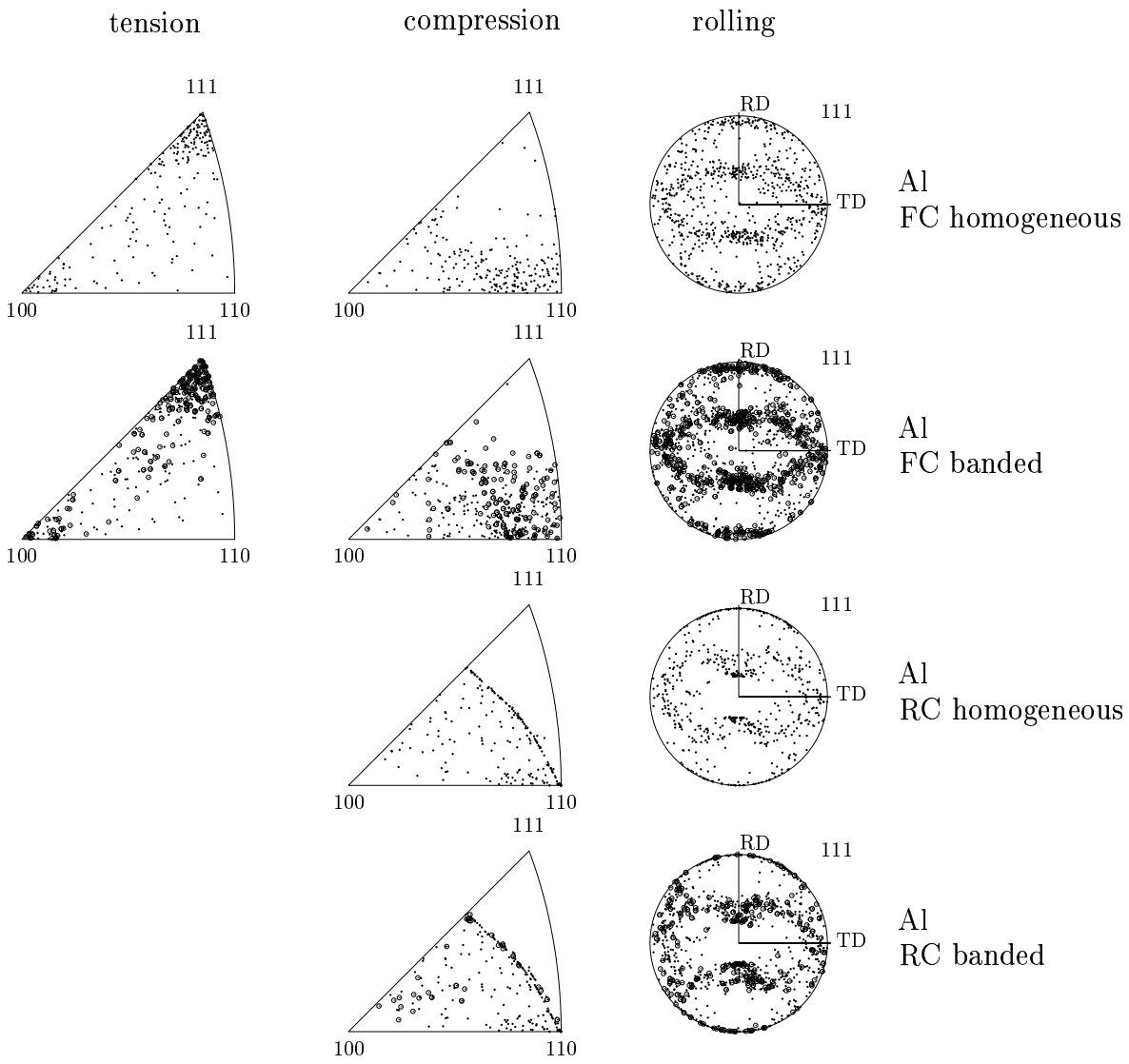

Figure 12: Inverse (tension and compression), and 111 direct pole figures (rolling) for aluminium after strain $|\epsilon_{11}| = 0.5$. The columns correspond to the different loadings as indicated. The rows correspond to FC and RC simulations with or without banding, as indicated. Since RC approximates tension poorly, that calculation is omitted. Open circles: grains with $0 \leq w < 0.5$; dots: grains with $0.5 \leq w \leq 1$.

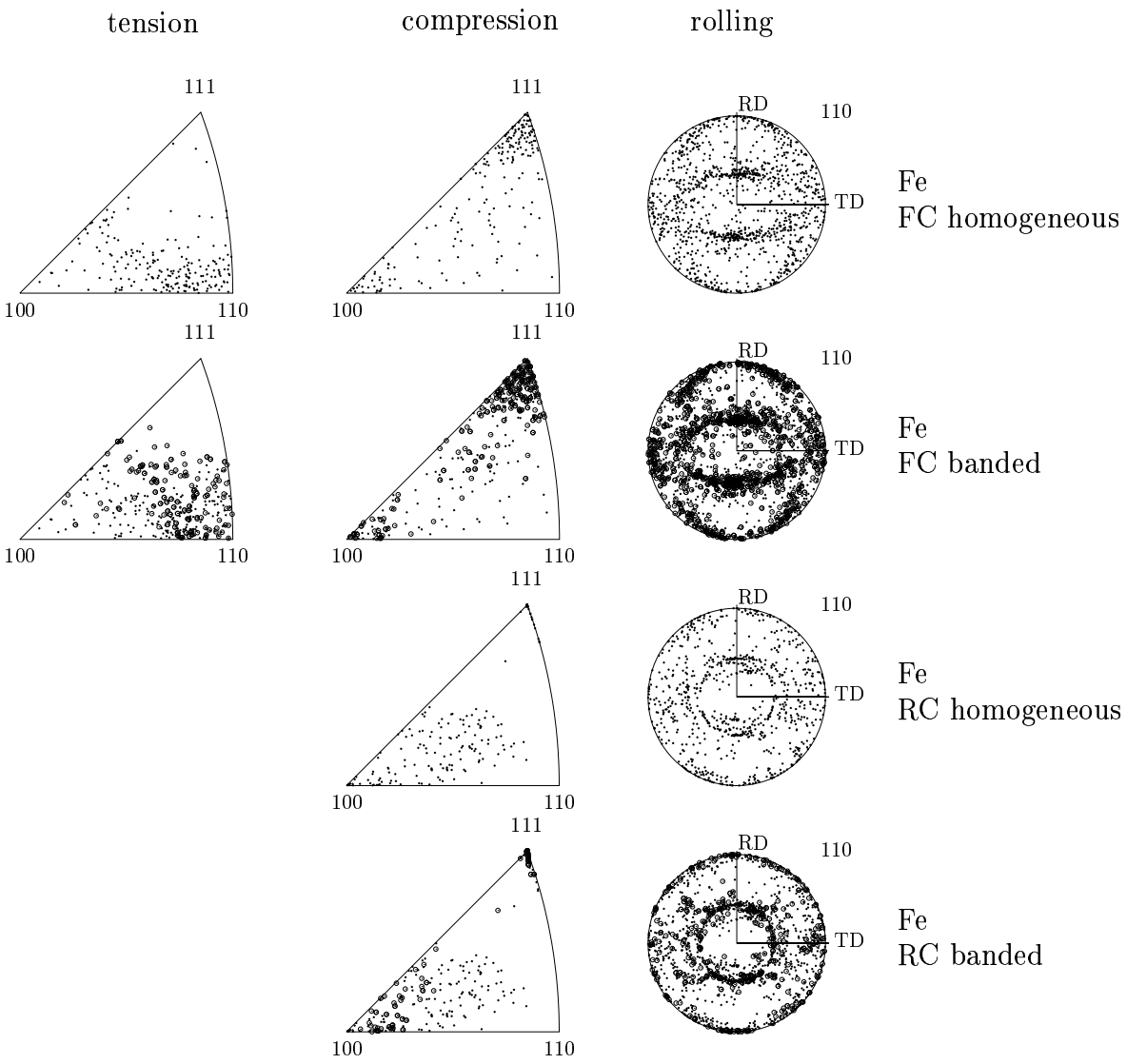

Figure 13: Inverse (tension and compression), and 110 direct pole figures (rolling) for iron after strain $|\epsilon_{11}| = 0.5$. The columns correspond to the different loadings as indicated. The rows correspond to FC and RC simulations with or without banding, as indicated. Since RC approximates tension poorly, that calculation is omitted. Open circles: grains with $0 \leq w < 0.5$; dots: grains with $0.5 \leq w \leq 1$.

List of Tables

Parameter	ref	Al	α-Fe
n	Eq. (9)	20	20
k_ω [°]	Eq. (17)	1	1
r	Eq. (21)	4	4
c	Eq. (21)	0.2	0.2
D [m]	Eq. (30)	$4 \cdot 10^{-4}$	$4 \cdot 10^{-4}$
κ_b	Eq. (48)	0.025	0.025
κ_c/D_0^2 [m^{-1}]	Eq. (52)	10^3	10^3
Gb [MPa m^{-1}]	various	$1.25 \cdot 10^{-5}$	$2.31 \cdot 10^{-5}$
θ_0 [MPa]	Eq. (33)	30.0	170.0
θ_1 [MPa]	Eq. (33)	0.5	3.0
τ_0 [MPa]	Eq. (33)	3.5	18.0
τ_1 [MPa]	Eq. (33)	19.0	87.0

Table 1: The model parameters as fit to the tensile experimental stress-strain curve for aluminium and α-iron.

Loading		Aluminium		Iron	
		Banded	Not banded	Banded	Not banded
FC	Tens	5.819	6.214	5.926	7.255
	Comp	5.958	7.257	5.812	6.214
	Roll	4.576	5.403	4.515	5.393
RC	Comp	4.542	4.599	5.265	5.266
	Roll	4.115	4.131	4.226	4.272

Table 2: Average number of active slip systems, $\langle n_{\text{active}} \rangle$ at strain $|\epsilon_{11}| = 0.5$ under the different loading conditions, and different constraints. Note that for a viscoplastic grain (Eq. (9)), $\langle n_{\text{active}} \rangle$ values in excess of 5 are permissible.